RECIRCULATING LOOP TESTBED FOR ALL-OPTICAL 2R REGENERATION

by

PALLAVI GOVIND PATKI

Presented to the Faculty of the Graduate School of

The University of Texas at Arlington in Partial Fulfillment

of the Requirements

for the Degree of

MASTER OF SCIENCE IN ELECTRICAL ENGINEERING

THE UNIVERSITY OF TEXAS AT ARLINGTON

August 2006

ACKNOWLEDGEMENTS

I would like to express my gratitude to my supervising professor Dr. Michael Vasilyev for his patience and guidance in completing this thesis. I have learnt a lot from him during my coursework as well as working with him in the lab. I am extremely thankful for his confidence in me and encouraging me during the course of this thesis.

I would like to express my gratitude to my parents and sisters for their unbounded care and love. Their encouragement was extremely valuable to me. Furthermore, I am thankful to Dr. Chiao, Dr. Stelmakh and Dr. Zhou for willing to be on my supervising committee.

I am grateful to my friend Harish, without whose support I would not have pursued my graduate studies. I would also like to thank my friends Smitha, Geetha, Karuna, Naren, Rajvi, Pooja, Shaan, and Anup for their support throughout the research. I would like to express my gratitude to my lab members Muthu, Sharath, and Veronika for their help and suggestions. I would like to thank all the members of NanoFAB for their help.

July 24, 2006

ABSTRACT

RECIRCULATING LOOP TESTBED FOR ALL-OPTICAL 2R REGENERATION

Publication No. _____

Pallavi Govind Patki, M.S.

The University of Texas at Arlington, 2006

Supervising Professor: Michael Vasilyev

This Master's thesis deals with building a recirculating loop testbed intended for proof-of-principle demonstration of multichannel all-optical 2R regenerator proposed in [1].

The proposed multichannel 2R regeneration scheme uses multiple highly-nonlinear-fiber (HNLF) sections separated by dispersion-compensating periodic-group-delay devices (PGDDs). The high cost and limited availability of these devices restrict us to working with just one PGDD, instead of 16 required by the scheme. Thus, for the proof-of-principle demonstration of the regenerator we have to put a single PGDD and a piece of HNLF into a recirculating loop through which light will circulate for required number of times.

In this thesis, we build and experimentally demonstrate the operation of the recirculating loop. This work has required building RZ and NRZ transmitter modules, coupling standard single-mode fiber (SSMF) to dispersion-compensating fiber (DCF, which we use as HNLF) and finally using them in the loop setup along with the other lab components and devices. The thesis describes the two transmitter sub-systems that we have built using JDS and Lucent modulators. We also discuss in detail the optimized bridge splicing technique used to couple SSMF to DCF. Finally, we present the design and experimental realization of our recirculating-loop testbed and trigger settings for the successful operation of the loop.

TABLE OF CONTENTS

LIST OF ILLUSTRATIONS

LIST OF TABLES

Table Page

CHAPTER 1

INTRODUCTION

The capacity and reach of optical networks is limited by a combined effect of amplifier noise accumulation, chromatic and polarization-mode dispersion, fiber nonlinearity, interchannel crosstalk, multipath interference, and other impairments. These degradations can be mitigated in two ways. The first way is conventional electronic regeneration, which consists of optoelectronic repeaters (transceivers or Tx/Rx pairs) periodically placed along the transmission link. This is a very costly as well as power- and space-hungry approach, as it requires separate repeaters for different WDM channels. The second solution is inline all-optical regeneration. Optical regeneration performs the same signal-restoring functions as the electronic approach, but with far reduced complexity and enhanced capabilities. Optical regeneration is classified as: 1R (reamplifying), 2R (reamplifying + reshaping), and 3R (reamplifying + reshaping + retiming). All-optical regeneration has been recognized as a potential enabler of future ultralong-reach high-bit-rate systems and all-optical packet-switched networks [2]. In Ref. [3], a simple all-optical fiber-based 2R regeneration technique was proposed. Here, the signal propagates through a piece of highly nonlinear fiber (HNLF) which causes the signal spectrum to broaden due to self-phase modulation (SPM). Then, the broadened spectrum is filtered out by an optical band pass filter (OBPF) whose

frequency is shifted with respect to the input signal. This method suppresses the noise in "zeros" and the amplitude fluctuations in "ones" of return-to-zero (RZ) optical data streams [3]. However, with this design simultaneous multichannel regeneration remains a challenge as it relies on strong nonlinear optical effects which cause the cross-talk among the WDM channels.

The solution to multichannel all-optical 2R regeneration has been proposed by our group in collaboration with Prof. T. I. Lakoba from the University of Vermont in [1], and its experimental realization is pursued in our lab. The approach [1] uses multiple HNLF sections with high normal dispersion, separated by dispersion compensating periodic-group-delay devices (PGDDs). PGDDs are the key components of our proposed generation scheme, and even the proof-of-concept demonstration of this regenerator requires at least 16 PGDDs. However, PGDDs are very expensive and are currently available only in a form of pre-commercial prototypes. We have managed to obtain a single PGDD from Avanex and hence will have to carry out the regeneration experiment with just one PGDD. For the proof-of-principle demonstration, we will put a single PGDD and a piece of HNLF into a recirculating loop through which light will pass multiple times.

This thesis focuses on building the recirculating loop required for the regeneration experiment. This effort has required designing and assembling several custom sub-systems and combining them with other commercial components and devices into a working setup. As the first step, we have built a transmitter module operating at rates up to and including 10 Gb/s, which required external modulators. In

our lab, we have had two commercial electro-optic modulators from JDS Uniphase and Lucent, respectively. Using these modulators, we have built a JDS-modulator-based RZ transmitter sub-system and a Lucent-modulator based NRZ transmitter sub-system. The second critical step has required a HNLF (in our case, it is dispersion-compensating fiber, or DCF), where the good coupling between this fiber and a standards single-mode fiber (SSMF) becomes of paramount importance. We have conducted a thorough optimization of splicing between the SSMF and DCF using Fujikura FSM-40PM Arc Fusion Splicer in our lab. Bridge splice technique has been used to combine these two fibers, wherein SMF-LS was employed as an intermediate bridge fiber. We have achieved better than 0.6 dB loss in coupling between the SSMF and DCF. As the third step, we have assembled and demonstrated the operation of the recirculating loop testbed to be used in 2R regeneration experiments, as well as in other future studies of optical communication devices, systems, and networks.

The thesis structure is as follows. In the first chapter of this thesis we explain in detail the working of external lithium niobate ($LiNbO_3$) interferometric Mach-Zehnder modulator (MZM). We discuss the RZ transmitter operation and describe in detail the transmitter sub-systems that we have built using JDS and Lucent modulators. We also discuss different modulation formats realizable with our modulators. The second chapter deals with coupling of SSMF to DCF. It describes in detail the optimized bridge splicing technique used to achieve this coupling. In the third chapter, we discuss the experimental setup of the recirculating-loop testbed constructed in our lab. We also explain the trigger settings used for successful operation of this loop. The last chapter

summarizes the thesis. In the appendix, we attach the specifications of several critical components used in our setup.

This research has been supported in part by the National Science Foundation (grant number DMS-0507540) and Lockheed Martin Corporation. We also acknowledge generous support from Corning Incorporated which provided transmission and DCF fibers for our experiments.

CHAPTER 2

MODULATION

2.1 Introduction

The first step in the design of any optical communication system is to superimpose the information signals onto an optical carrier, i.e. to convert the electrical signal into an optical bit stream. This is achieved by optical modulators. There are two basic techniques used to modulate an optical carrier: Direct Modulation and External Modulation.

2.1.1 Direct Modulation

In direct modulation, the electrical signal applied to the power terminals of the laser source directly modulates the laser gain. A basic advantage of this approach is its inherent simplicity. However, at bit rates of 10 Gb/s and higher, undesirable optical frequency variations, referred to as frequency chirp become very large [4]. Another limiting factor to direct modulation is the relatively long time response of the laser diode and its electronic driving circuit. Thus, for high-speed transmitters external modulation is required.

2.1.2 External Modulation

In external modulation, the semiconductor laser's output is passed through a separate device, called external modulator, which modulates the optical carrier. In external modulators, the laser source is biased at constant current to provide the

continuous wave (CW) output, and a high-speed optical modulator is placed next to the laser. This external modulator then converts the CW light into a data-coded pulse train with appropriate modulation format. With external modulation, transmitter design becomes more complex, requiring additional expensive components. However, external modulation is the preferred method for high-speed communication as it avoids excessive spectral broadening and frequency chirping resulting in serious dispersion and crosstalk problems inherent to direct-modulated lasers. Key features of external modulators that make them attractive for this application are their broad modulation bandwidth, large extinction ratio, excellent spectral purity of the transmitted signal, high optical power handling capability, low modulation distortion, and fabrication yield and reproducibility.

Two main classes of external optical modulators are electro-absorption (EA) modulators, and electro-optic (EO) modulators. The former are typically used at 10 Gb/s and lower rates and are often monolithically integrated on the laser diode chip. The latter are used at 10 Gb/s and higher rates, since at lower rates less expensive approaches are possible. In UTA testbed, the focus is on 10 Gb/s and beyond, hence we will concentrate on the description of EO modulators. The EO modulator works on the principle of electro-optic effect. While, in general, this effect can be to some extent observed in all materials, only linear electro-optic effect inherent to non-centro-symmetric crystals, such as lithium niobate ($LiNbO_3$) is of practical interest to high-speed communcation. In this case, the refractive index of the material changes linearly in response to an applied electric field. Since the refractive index is inversely

proportional to the velocity of light, change in refractive index causes a corresponding change in light velocity. Thus, by varying the refractive index, the velocity of light beam propagating through such materials can be changed. Electro-optic modulator of interest in high-bit-rate, long-haul communication systems is the popular $LiNbO_3$ interferometric Mach-Zehnder Modulator (MZM). $LiNbO_3$ crystals are traditionally used to manufacture these modulators as they exhibit particularly strong linear electro-optic effect. Next section focuses on the operation principle of the external MZM.

2.2 The External Interferometric Mach-Zehnder Modulator (MZM)

The $LiNbO_3$-based MZM has become popular choice in high-bit-rate, long-haul communication systems because of its wide bandwidth, relatively small absorption and coupling losses, and potential for integration with other photonic components on a single $LiNbO_3$ chip.

MZM modulators can be used either as phase or as amplitude modulators. One way to implement a MZM is a dual-electrode dual-drive configuration shown in Fig. 2.1. The dual-drive modulator can achieve either phase or amplitude modulation, or even a combination of the two. However, this advantage comes with a drawback, as it is requires precise match of amplitude and phase responses of two electronic amplifiers driving the two electrodes. The dual-drive MZM consists of a single optical input of polarization-maintaining (PM) fiber, a Y-junction (50/50 beam splitter), two phase-modulated waveguides (arms) with independent drive electrodes, an output Y-junction (50/50 combiner), and a single optical output of PM or single-mode fiber (SMF). The two electrodes allow injection of two independent RF signals into the modulator. The

input optical signal with amplitude E_0 is split at the first Y-junction into the two arms of the modulator with amplitudes $E_0/\sqrt{2}$. Voltages applied to the electrodes positioned either next to or on top of the waveguides introduce phase shifts in both arms. Thus, if $V_1(t)$ and $V_2(t)$ are the voltages applied to the two electrodes, then light will be phase-shifted by amounts $\theta_1(t)$ and $\theta_2(t)$ in the two arms of the modulator.

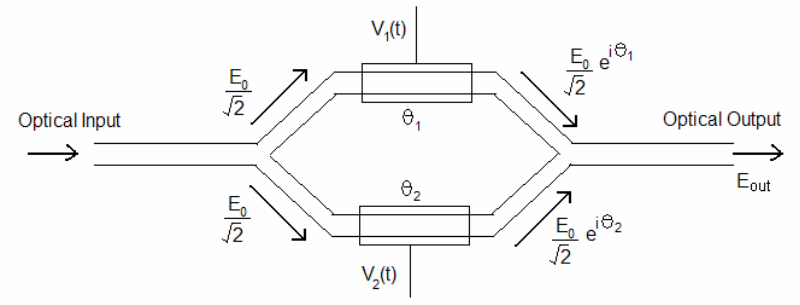

Fig. 2.1. Schematic diagram of $LiNbO_3$ Mach-Zehnder modulator.

The amplitude of the modulated light can be expressed as:

$$
\begin{aligned}
E_{\text{out}} = \text{Modulator Output} &= \left(\frac{E_0}{\sqrt{2}}e^{i\theta_1} + \frac{E_0}{\sqrt{2}}e^{i\theta_2}\right)\frac{1}{\sqrt{2}} \\
&= \frac{E_0}{2}\left(e^{i\theta_1} + e^{i\theta_2}\right) \\
&= \frac{E_0}{2}\left[e^{i\left(\frac{\theta_1}{2}+\frac{\theta_2}{2}+\frac{\theta_1}{2}-\frac{\theta_2}{2}\right)} + e^{i\left(\frac{\theta_1}{2}+\frac{\theta_2}{2}+\frac{\theta_2}{2}-\frac{\theta_1}{2}\right)}\right] \\
&= E_0\left[\frac{e^{i\left(\frac{\theta_1+\theta_2}{2}\right)}e^{i\left(\frac{\theta_1-\theta_2}{2}\right)}}{2} + \frac{e^{i\left(\frac{\theta_1+\theta_2}{2}\right)}e^{i\left(\frac{\theta_2-\theta_1}{2}\right)}}{2}\right] \\
&= E_0 e^{i\left(\frac{\theta_1+\theta_2}{2}\right)}\frac{e^{i\left(\frac{\theta_1-\theta_2}{2}\right)} + e^{i\left(\frac{\theta_2-\theta_1}{2}\right)}}{2} \\
&= E_0 e^{i\left(\frac{\theta_1+\theta_2}{2}\right)}\cos\left(\frac{\theta_1-\theta_2}{2}\right).
\end{aligned}
\tag{2.1}
$$

If equal voltages are applied to both arms, then $\theta_1=\theta_2=\theta$. The modulator output in equation (2.1) can now be expressed as:

$$E_{\text{out}}=E_0 e^{i\theta(t)} , \tag{2.2}$$

i.e. the modulator performs pure phase modulation.

If the modulator arms are driven by voltages with equal magnitude but opposite polarity, i.e. $V_1(t) = -V_2(t)$, then $\theta_1= -\theta_2 = \theta$ and the modulator output is given by

$$E_{\text{out}}=E_0 \cos\theta(t) . \tag{2.3}$$

In general, if $V_1(t)$ and $V_2(t)$ are adjusted such that the phase-shift difference between the two arms is an odd multiple of π, the two light beams will cancel (extinct) at the beam-combiner output. The amount of extinction depends on the ideality of the modulator, which depends on how equally light has been divided into the two arms of the modulator, how well the polarization has been maintained in the device, etc. The voltage applied to the electrodes changes the phase of light in each arm, which causes the output optical amplitude to vary as the light recombined from the two paths moves from constructive to destructive interference. Therefore, MZM achieves intensity modulation via phase modulation. If the phases are exactly equal in magnitude in each path but are different in sign, the modulator is referred to as 'chirp-free,' which means that the output is purely intensity modulated [as shown in equation (2.3)] without incidental phase modulation.

Several important parameters that determine the performance of a modulator are [5]:

1. *Bandwidth* is related to the maximum speed at which the modulator performs on/off operation efficiently.

2. *Drive Voltage* (V_π) is the voltage that achieves a phase difference of π between the two arms and hence results in shift from perfect addition of the two light beams to complete cancellation of light at the modulator output. An electrically efficient modulator should have a value of V_π as small as possible.

3. *Bias Voltage* (V_b) is the DC voltage around which the modulation signal swings.

4. *Optical Insertion Loss* (IL) characterizes the amount of light that is passively lost (i.e. not through the process of modulation) due to propagation from one end of the modulator to the other. It is usually expressed in decibels as 10 $\log_{10}$ (input power / output power) under the constructive interference conditions. Higher optical losses translate into less light available to transport the information.

5. *Modulator Chirp* describes the change in wavelength (frequency) of the light beam, caused by on/off operation of the modulator. Consequently, as the chirped pulse of light propagates through the dispersive fiber, it is significantly more distorted than a chirp free pulse. In addition, this effect limits the spectral efficiency of the optical transmission system by increasing the signal bandwidth.

6. *Optical Extinction Ratio* (ER) describes the ability of modulator to extinguish light when the modulator is driven to an off state and is expressed in decibels as 10 $\log_{10}$ (power in “on” state / power in “off” state).

2.3 $LiNb0_3$ MZM: Electrode Configuration and Fabrication

In high speed digital communication applications, fiber dispersion is one of the factors limiting system performance. $LiNbO_3$ external modulators provide both the required bandwidth and the equally important means for minimizing the effects of dispersion. Unlike direct modulation of a laser diode, $LiNbO_3$-based guided-wave modulator can be designed for zero-chirp or adjustable-chirp operation. Zero-chirp and negative-chirp modulators help to minimize the system degradation associated with the fiber dispersion. Advances in $LiNbO_3$ modulator technology have enabled stable operation over temperature, very low bias-voltage drift rates and bias-free devices [6]. In this section, an overview of $LiNbO_3$ modulator is given.

Lithium niobate has been the material of choice for the fabrication of electro-optic modulators. Apart from exhibiting strong electro-optic effect, $LiNbO_3$ has other advantages for being used in fabrication of modulator waveguide. It is thermally, chemically and mechanically stable and is compatible with the conventional integrated-circuit processing technology. $LiNbO_3$ wafers with diameters up to 100 mm are commercially available in different crystal cuts (*x*-, *y*-, and *z*-cuts) [6]. RF electrodes are fabricated either directly on the surface of the wafer or on an optically transparent buffer layer. In general, an adhesion layer such as Ti is first deposited on the wafer, followed by the deposition of a base layer of the metal from which the electrodes are to be made. The electrode pattern is then photo-lithographically defined. High-speed modulators incorporate RF electrodes whose thickness can range from a few micrometers to greater than 15 μm [6]. Due to crystal symmetry in $LiNbO_3$, there are

two useful crystal orientations (*z*-cut and *x*-cut) which take advantage of the strongest electro-optic coefficient for the modulating electric field aligned with *z*-axis [6]. Figure 2.2 shows the electrode configurations for *x*- and *z*-cut devices.

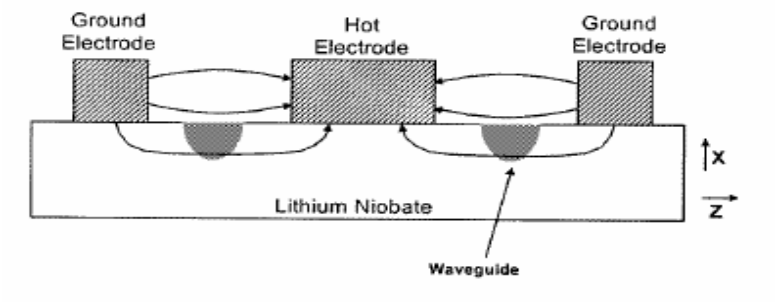

(a)

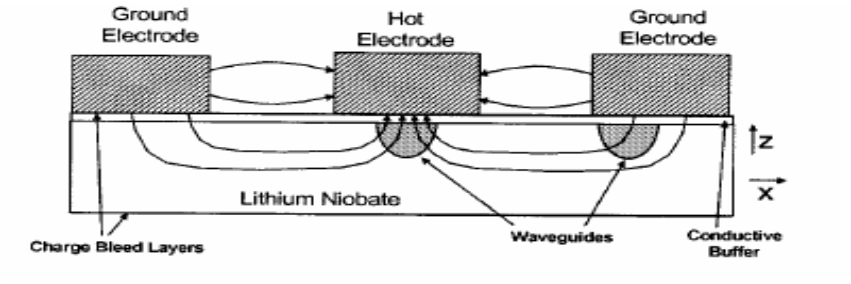

(b)

Fig. 2.2. Electrode configuration for (a) nonbuffered *x*-cut, (b) buffered single-drive *z*-cut [6].

A *z*-cut device uses the vertical component of the modulating electric-field, and an *x*-cut device uses the horizontal component. The first choice encountered in designing a $LiNbO_3$ modulator is orientation of the crystal axes to the waveguides and electrodes. The strongest component of the applied electric field must be aligned with the *z*-axis of the crystal, which has the highest electro-optic coefficient. This requires that the waveguide be placed between the electrodes for an *x*-cut configuration and beneath the electrodes for *z*-cut [6]. As electrodes are placed on top of the waveguides

in *z*-cut devices, it is necessary to have a buffer layer (isolation layer) between the two in order to avoid increased optical losses due to metal loading. Buffer layer is not required in *x*-cut devices as the electrodes are not placed directly above the waveguides.

2.4 Modulation Formats

It is vital to choose an appropriate modulation format to achieve good system performance while transmitting signals in high-speed WDM communication systems. The simplest modulation format is on-off-keying (OOK) intensity modulation, which can take either of two forms: non-return-to-zero (NRZ) or return-to-zero (RZ). Figure 2.3 illustrates the RZ and NRZ coding for the same data sequence 1 1 1 0 0 1 0 1 0 1 1 1.

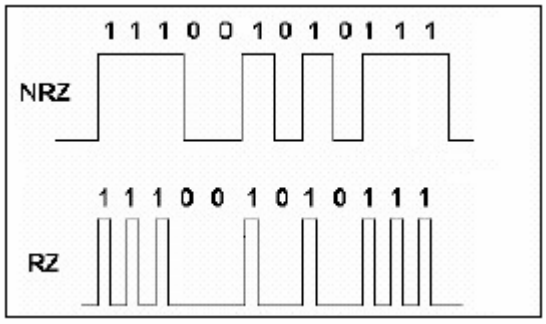

Fig. 2.3. NRZ and RZ coding for 111001010111 data stream.

2.4.1 NRZ modulation format

In a conventional NRZ modulation format, “0” is represented by low logic level and “1”—by high logic level that does not return to zero between consecutive “1” bits. Thus in NRZ, the input data rate determines the pulse width. NRZ is relatively easy to implement, less costly and needs the signal bandwidth which is half the bandwidth

required by RZ format, which makes it the preferred choice for bit rates below 10 Gb/s and for metropolitan area networks. However, NRZ is more susceptible to “bit-pattern-dependent” effects due to optical pulse spreading during propagation. Hence there is a need for rigid control of dispersion and nonlinearity at higher bit rates.

2.4.2 RZ modulation format

In the RZ format, “ones” are represented by a high logic level that returns to “zero” between consecutive “one” bits. For this reason, RZ format requires two transitions (high-low) per bit, which result in larger bandwidth compared to NRZ. Since RZ creates distinct pulse encoding of the bit, it is less susceptible to pattern dependence caused by dispersion and nonlinearity. For the same average power as NRZ, the pulse’s peak power is higher, leading to better receiver sensitivity than the NRZ. Owing to these advantages, RZ modulation has become predominantly popular with high-speed lightwave systems such as ultra-long-haul 10 Gb/s and 40 Gb/s [7, 8], where the effects of dispersion and nonlinearity are prominent.

2.4.3 Advanced modulation formats

The simple NRZ and RZ modulation formats are a natural choice when the bandwidth is plentiful and the dispersion and nonlinearities are well controlled [8]. Otherwise, the ultra-high speed systems working with RZ signal transmission may encounter symbol interference between the neighboring bits (intersymbol interference), or ISI. Hence sophisticated modulation formats are needed to provide benefits like improved receiver sensitivity, higher tolerance to nonlinear effects, improved dispersion tolerance and

possibility of closer channel spacing [8]. However, it is extremely difficult to get all the above mentioned features in a single format, hence the system designers select the modulation format depending on the application. Here, we briefly mention two of the advanced modulation formats, carrier-suppressed RZ (CS-RZ) and duo-binary coding.

2.4.3.1 Carrier Suppressed RZ (CS-RZ)

As the name implies, CS-RZ optical signal has no carrier component and hence it is less sensitive to certain nonlinearities (e.g. Stimulated Brillouin Scattering). In addition, CS-RZ occupies narrower bandwidth than RZ, thereby enabling tighter WDM channel spacing. The CS-RZ signal is obtained by introducing a phase shift of π between consecutive pulses, which also reduces intersymbol interference. It can be implemented with the same dual-modulator configuration as that used for RZ format, to be discussed in Section 2.5, where the pulse carver is operated at half the bit rate with twice the peak-to-peak voltage (i.e. $2V_\pi$) and the modulator is biased at minimum transmission ($V_b = V_\pi$) to produce optical pulses with 67% duty cycle [8].

2.4.3.2 Optical duo-binary format

A duo-binary modulation format uses three different physical levels, E, 0, and $-E$ to represent 1, 0, −1, where E is the optical field amplitude. This facilitates duo-binary signal to be more tolerant to ISI distortion, as bit patterns, for instance 1 0 1 are transmitted with ones carrying an opposite phase (i.e. the corresponding optical amplitude is either E 0 $-E$ or $-E$ 0 E). Thus, if the pulses corresponding to the 1 bits spread out into the 0 time-slot in between due to fiber dispersion, they tend to cancel out each other [8].

2.5 RZ Transmitter

A conventional RZ transmitter system mainly consists of three optical components: a continuous-wave laser source, one lithium niobate MZM for pulse generation, referred to as "pulse carver," and another lithium niobate MZM for encoding data on this generated pulse train. Each modulator is accompanied by a voltage driver amplifying the RF modulating signal to level of the order of V_π. Figure 2.4 shows the traditional RZ transmitter. The continuous-wave light from a distributed-feedback (DFB) laser source is input to the first MZM driven by a sinusoidal signal, either at full- or half-clock frequency, to produce a periodic RZ pulse train. If directly driven at the clock frequency, the modulator is biased at its transmittance midpoint and is driven by V_π /2-amplitude sine wave to provide full on/off output. If the modulator is driven at half the clock frequency, it is biased at a peak or a null, and is driven between two adjacent nulls or peaks, respectively, at twice the voltage. The half-clock-frequency approach results in narrower pulses because of the sinusoidal transfer function of the EO MZM. In either case, the output of the first modulator is a pulse train at the bit rate. This pulse train then enters the second MZM encoding the data on it by blocking some of the pulses.

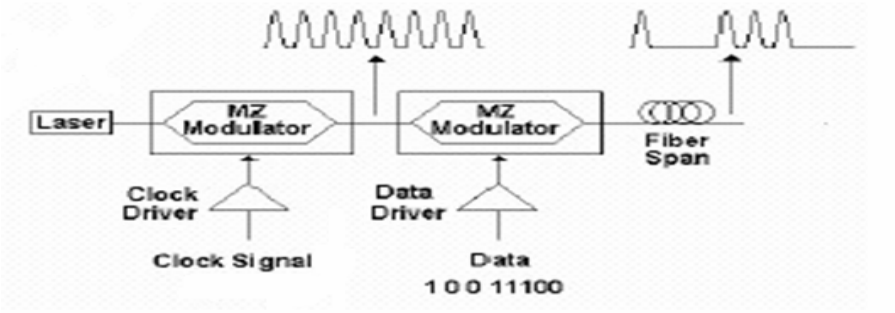

Fig. 2.4. Typical RZ transmitter [9].

To reduce the IL of two cascaded MZMs used for RZ signal generation, the commercial RZ transmitters integrate both MZMs on the same $LiNbO_3$ substrate, thereby eliminating fiber coupling losses between them. Figure 2.5 shows a RZ transmitter implemented using two-stage $LiNbO_3$ device. The ability to integrate multiple functions on a single chip has been a powerful attribute of $LiNbO_3$ technology.

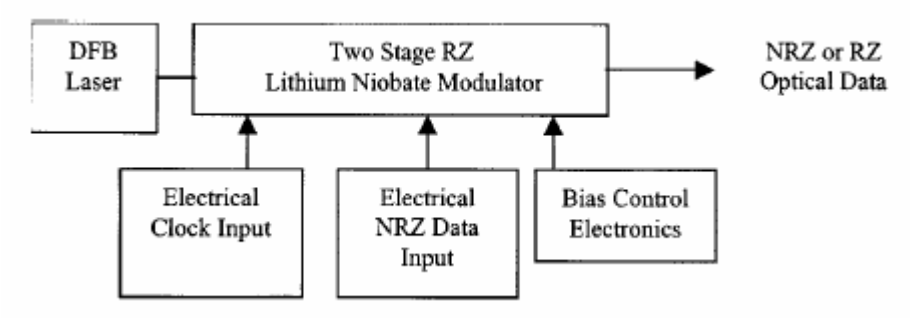

Fig. 2.5. Schematic showing pulse-data modulator architecture for RZ transmission [5].

2.6 Duty cycle of generated RZ pulses

With traditional 50% duty-cycle pulse generation, the bias of the pulse carver is set at the midpoint of linear region (quadrature point) of the MZM transmittance curve and the sinusoidal drive voltage at clock frequency, with $V_\pi/2$ amplitude is allowed to swing between the points of minimum and maximum transmittance [8], as depicted in Fig. 2.6(a). By decreasing the modulation swing and adjusting the bias point to anywhere between the midpoint and minimum point of the transmittance curve (i.e. lowering the bias point on the transmittance curve), shorter (smaller duty cycle) pulses can be generated as depicted in Fig. 2.6(b).

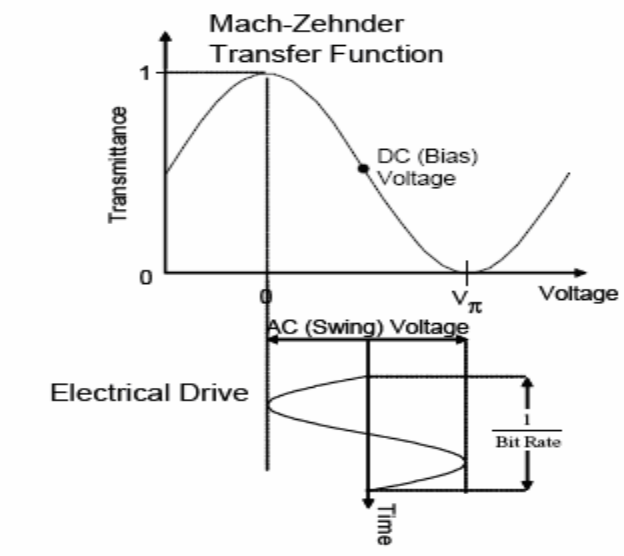

(a)

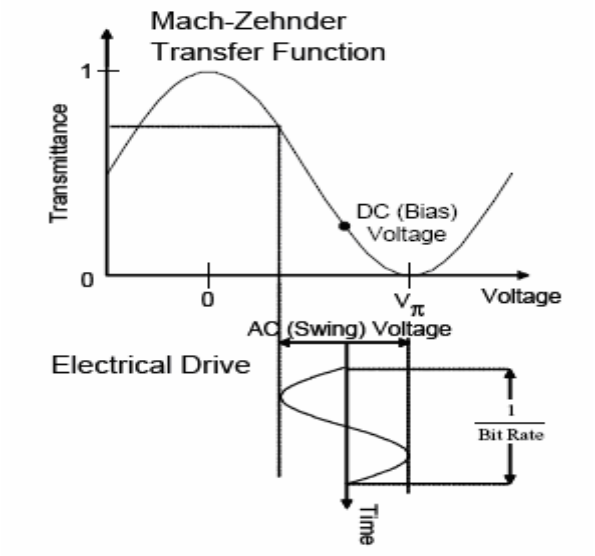

(b)

Fig. 2.6. Drive and bias voltage settings for the generation of (a) standard 50% duty cycle RZ pulses (b) 38% duty cycle pulses [10].

For the half-clock-frequency driving signal, two options are available:

(a) Modulator can be driven by a half-clock-frequency sine wave with amplitude of V_π and biased at the maximum, as shown in Fig. 2.7(a). In that case, 33%-duty-cycle pulses are generated [8, 10].

(b) When the MZM is driven with a half-clock-frequency sine wave with amplitude of V_π and biased at the minimum transmission, as shown in Fig. 2.7(b), CS-RZ pulses with 67% duty cycle are generated at the output of the modulator [8, 10], because neighboring maxima produce output fields with opposite phases.

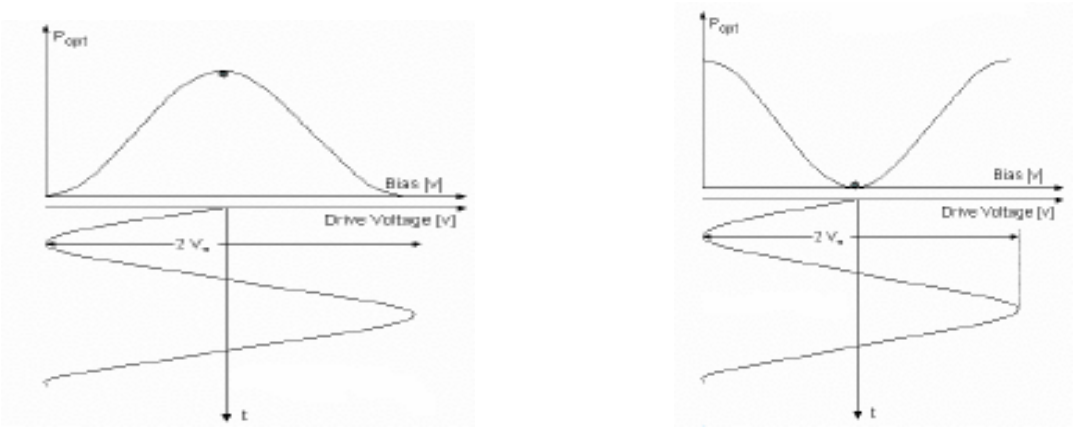

(a) (b)

Fig. 2.7. Generation of (a) RZ and (b) CS-RZ pulses by the pulse-carver modulator driven at half the clock frequency [11].

2.7 Lab Modulator

In our lab, we use two lithium niobate MZMs, one of which is manufactured by JDS (model number 10022802) and the other one by Lucent (model number X2625X0018). Figure 2.8 shows the block diagram of our 10 Gb/s JDS modulator-based transmitter

sub-system. The JDS modulator used here is a dual- stage MZM comprised of 10 Gb/s NRZ data modulator and RZ pulse carver stage.

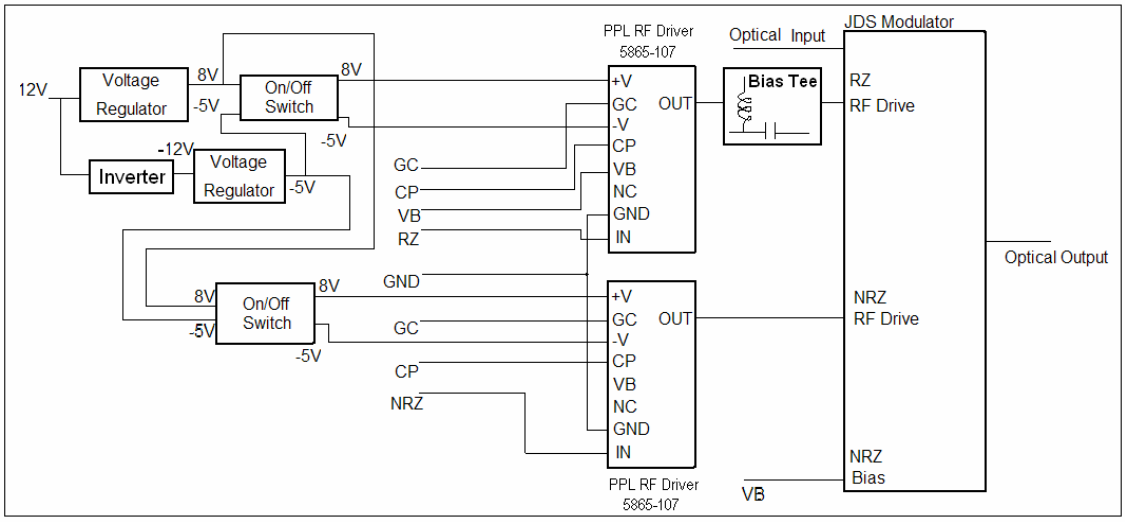

Fig. 2.8. Block diagram of JDS-modulator-based RZ transmitter sub-system.

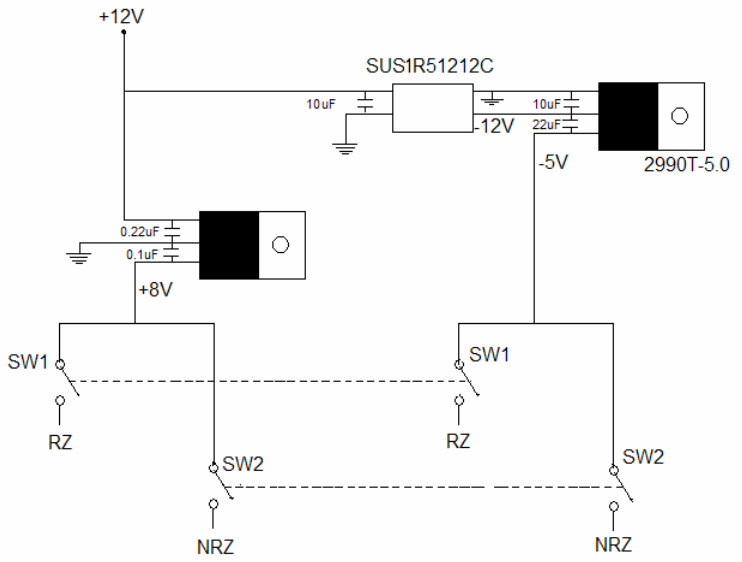

Fig. 2.9. Power supply section of JDS-modulator-based RZ transmitter sub-system.

Each modulator driver requires a positive DC voltage supply of +8V and negative supply of −5V. To provide this, we have built power supply circuit, depicted in

Fig. 2.9, which converts 12V from an inexpensive wall-pluggable DC adapter into stabilized +8V and −5V, respectively. Through this circuit, DC power supply is provided to each modulator.

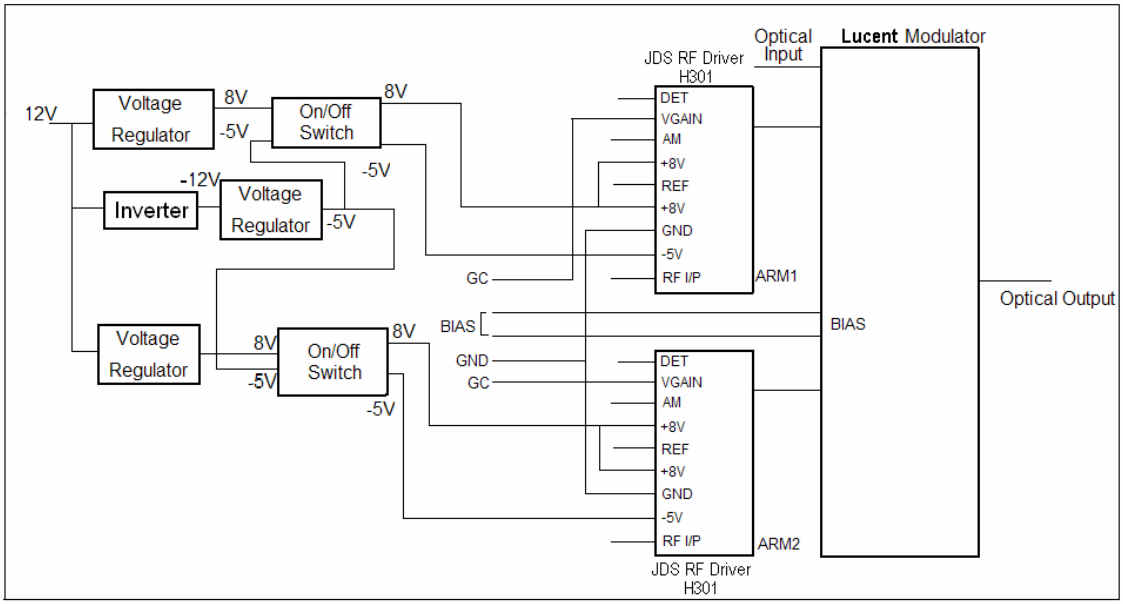

Fig. 2.10. Block diagram of Lucent-modulator-based NRZ transmitter sub-system.

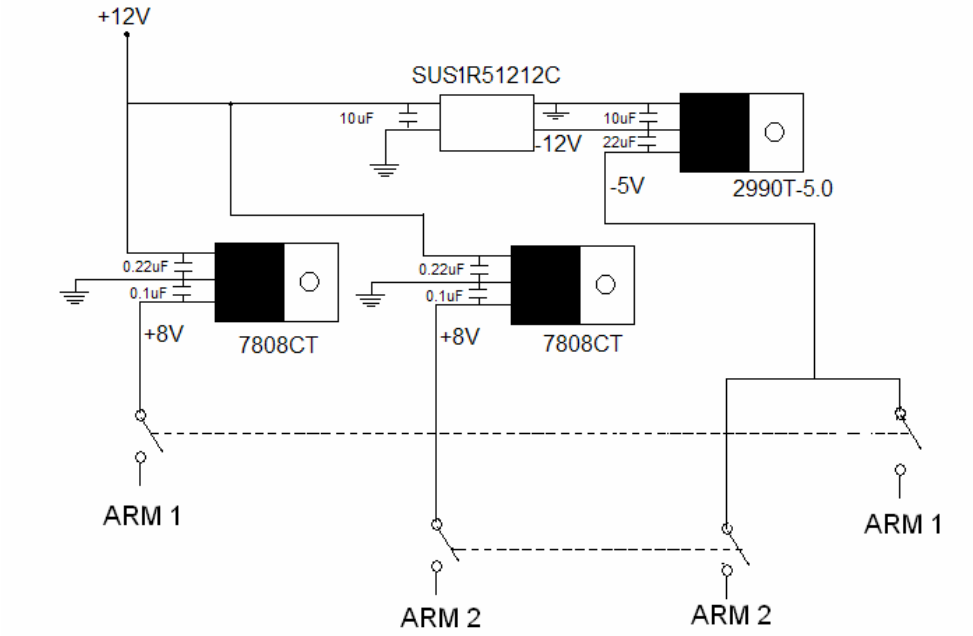

Fig. 2.11. Power supply section of Lucent-modulator-based NRZ transmitter sub-system.

Figure 2.10 shows the block diagram for 10 Gb/s RZ transmitter sub-system using Lucent modulator, and Figure 2.11 shows the schematic of the power supply section of Lucent modulator sub-system. While the Lucent modulator can work up to 40 Gb/s, our driver electronics only allows for operation up to and including 10 Gb/s. The modulator consists of only one stage; hence, only NRZ operation is possible. However, we can drive the two arms of the MZM independently, thereby achieving either intensity, or phase modulation, or the combination of the two (e.g. single-sideband modulation).

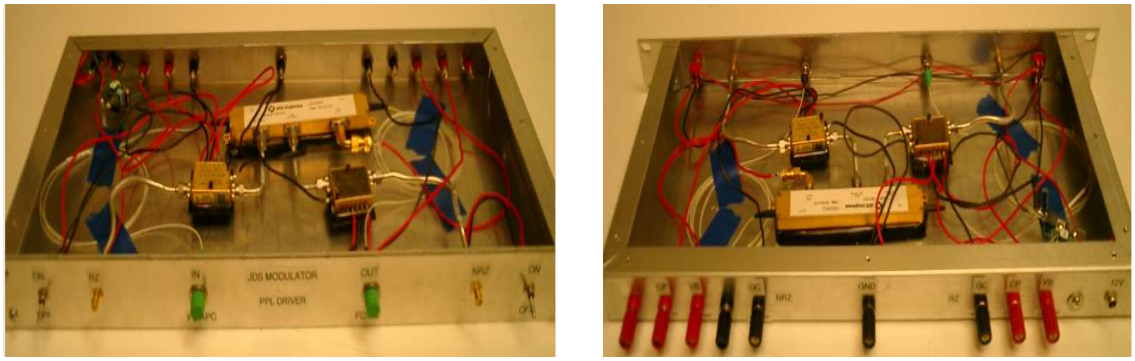

Fig. 2.12. JDS-modulator-based RZ transmitter sub-system.

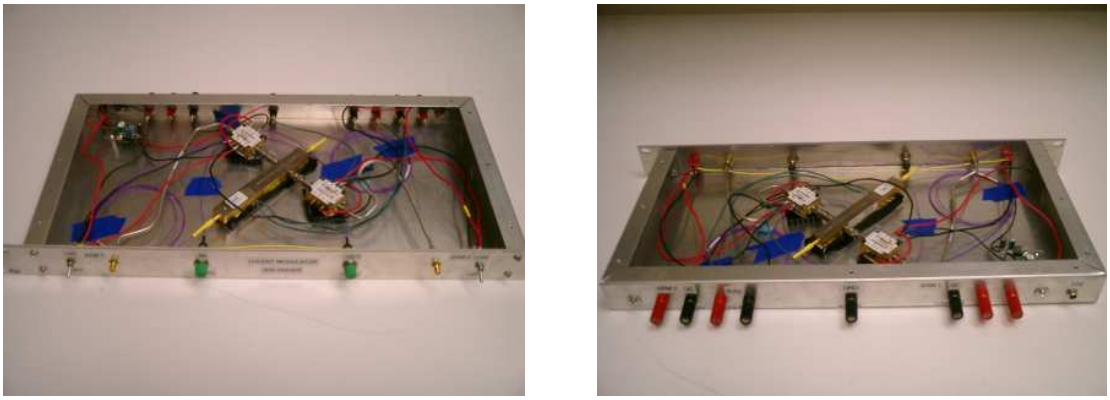

Fig. 2.13. Lucent-modulator-based NRZ transmitter sub-system.

Both JDS and Lucent modulators are fixed on the bottom of the corresponding rack-mounted aluminum boxes. Each box provides optical and RF inputs and outputs on the front panel and electrical connections (12V power, gain-control, bias, and cross-point voltages) on the back panel. Figures 2.12 and 2.13 show both modulator boxes with their front and back panels.

Picosecond Pulse Labs' 5865-107 RF drivers used in JDS-based sub-system allow for electronic control of their RF gain and crossing point, as well as provide an input for DC bias to be connected to the modulator in series with 2.5 kΩ resistor. We have found optimum settings under which no electronic gain or crossing-point adjustment is needed (the corresponding inputs are left open). For 9.95654 Gb/s bit rate, these settings are as follows:

RZ stage: CP = 0 V, GC = 0 V, Bias = 3.1 V (half-transmittance), RF input power = 2 dBm;

NRZ stage: CP = 0 V, GC = 0 V, Bias = 7.1 V (half-transmittance), driven by 6-dB-attenuated DATA output of the pattern generator set to Amplitude = 600 mV, Termination = 0 V DC, High level = 0 V.

NRZ bias is supplied to the separate bias port of the JDS modulator (NRZ RF port is AC coupled). On the other hand, RZ bias needs to be provided through RZ RF port using either driver's bias port or an external bias "T." We have found that, in our modulator's RZ section, the bias termination has been damaged and its impedance fluctuates wildly between tens of Ohms and infinity. As a result, using bias port of the driver becomes impossible, and we use the external bias "T" (Picosecond Pulse Labs'

5575A, not shown in Fig. 2.12). Even with this arrangement, the bias voltage across the modulator sometimes exhibits erratic behavior.

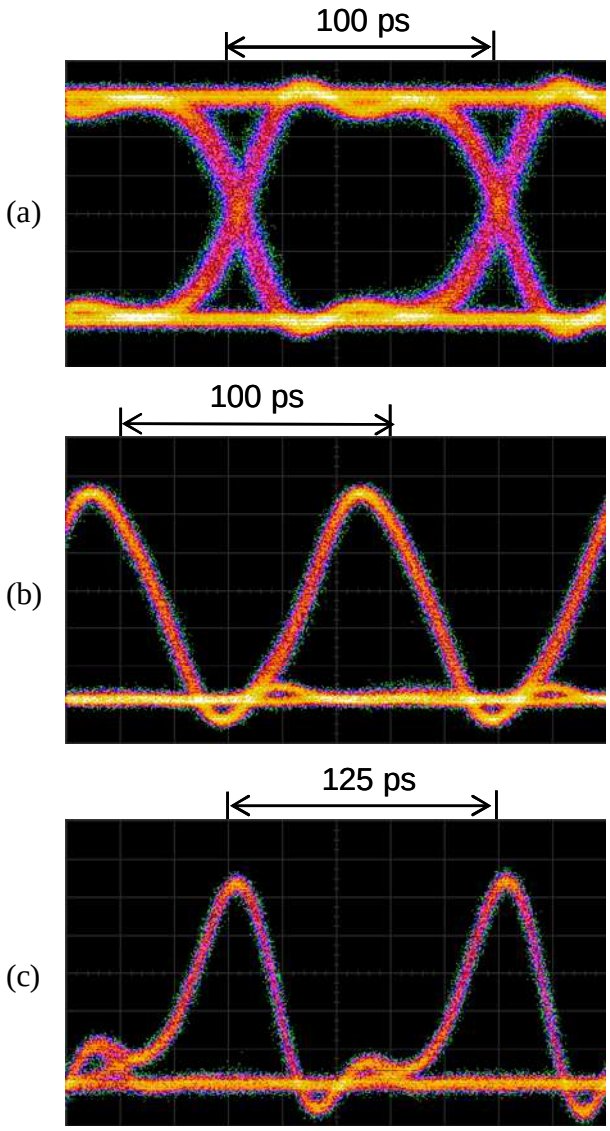

Fig. 2.14. Eye diagrams of JDS-modulator-based RZ transmitter sub-system showing three modulation formats: (a) NRZ at 10 Gb/s, (b) RZ at 10 Gb/s, and (c) CS-RZ at 8 Gb/s.

2.8 Modulator Results

Figure 2.14 shows the eye diagrams of NRZ, RZ and CS-RZ modulation formats generated using JDS-modulator-based transmitter. The generated NRZ format has extinction ratio (or ER) of 12.2 dB and Q-factor of 13.9. The RZ pulses are generated with 50% duty cycle and CS-RZ—with 33% duty cycle. Since CS-RZ requires higher driving voltage, we have put our RF drivers to their extreme of heavy saturation. As a result, we have obtained 33% CS-RZ duty cycle with some added distortion, as can be seen in Fig. 2.14(c), instead of 67% duty cycle expected for a modulator driven by linear RF amplifier.

In addition, electrically, the first stage of the JDS modulator ("pulse carver") represents a resonant circuit having maximum response around 10 GHz and zero response around 5 GHz. Thus, driving it at half clock frequency of 10 Gb/s signal (i.e. at 5 GHz) is impossible (for this, a separate modulator with finite 5 GHz response would be needed). To demonstrate CS-RZ operation, we have produced 8 Gb/s signal (pulse carver driven by 4 GHz) instead.

CHAPTER 3

COUPLING OF STANDARD SINGLE-MODE FIBER TO DISPERSION-COMPENSATING FIBER

3.1 Introduction

An optical signal transmitted through optical fiber suffers from linear and nonlinear degrading effects. While fiber dispersion and attenuation are the linear effects in optical fibers, self phase modulation (SPM), cross phase modulation (XPM), and four-wave-mixing (FWM) are the nonlinear effects. Dispersion and nonlinear effects are interrelated with each other. Increase in local dispersion of the transmission fiber decreases most of the effects of nonlinearity in optical fibers. Although large local dispersion is desirable in order to suppress the effects of nonlinearity, the resulting large accumulated dispersion itself is an important degrading effect and hence dispersion compensation becomes essential.

This chapter starts with a discussion of dispersion in single-mode fibers, followed by brief explanation of different types of optical transmission fibers based on their value of dispersion. It is then followed by the discussion of dispersion-compensating fiber (DCF), whose use requires attaching standard-single-mode-fiber (SSMF) pigtails to the DCF using bridge-splicing technique. The last section of this chapter elaborates on splice-loss optimization when splicing SSMF to SMF-LS and SMF-LS to DCF (bridge-splice), using fusion splicer in our lab.

3.2 Dispersion in Single-mode fibers

For single-mode fiber (SMF), the main source of dispersion is the Group-Velocity Dispersion (GVD). GVD in SMF comes from the fact that the refractive index of the optical fiber is a function of the wavelength, $n(\lambda)$. Therefore, a specific spectral component, with wavelength λ, traveling though a SMF of length L, would arrive at the output end of the fiber after a time delay of $T = L / v_g(\lambda)$, where $v_g(\lambda)$ is the group velocity. Since different spectral components associated with the pulse propagate with different speeds given by $v_g(\lambda) = c / n(\lambda)$, they do not arrive at the same time at the fiber output and hence lead to pulse broadening. This is commonly referred to as chromatic dispersion.

Mathematically, the effects of dispersion are accounted for by expanding the mode-propagation constant β [1/km] in Taylor series about frequency ω_0 at which the pulse spectrum is centered [4, 12]:

$$\beta(\omega) = n(\omega)\frac{\omega}{c} = \beta_0 + \beta_1(\omega-\omega_0) + \frac{1}{2}\beta_2(\omega-\omega_0)^2 + \ldots\ldots , \tag{3.1}$$

where $\beta_m = \left(\frac{d^m\beta}{d\omega^m}\right)_{\omega=\omega_0}$, (m=0, 1, 2….).

First derivative of equation (3.1) is given by

$$\frac{d\beta}{d\omega} = \frac{dn(\omega)}{d\omega}\cdot\frac{\omega}{c} + n(\omega)\cdot\frac{d}{d\omega}\left(\frac{\omega}{c}\right) \quad . \tag{3.2}$$

Therefore,

$$\beta_1 = \frac{d\beta}{d\omega} = \frac{\omega}{c}\frac{dn}{d\omega} + \frac{n}{c} = \frac{1}{v_g} \quad . \tag{3.3}$$

Second derivative of Eq. (3.1) can be obtained by differentiating Eq. (3.3) and is given by

$$\beta_2 = \frac{d^2\beta}{d\omega^2} = \frac{d}{d\omega}\left(\frac{1}{v_g}\right) = \frac{1}{c}\left(2\frac{dn}{d\omega} + \omega\frac{d^2n}{d\omega^2}\right) \quad . \tag{3.4}$$

In the above equations, c is the speed of light in vacuum, λ is the wavelength and ω is the frequency. The parameter β_2 is known as the GVD parameter. It determines how much an optical pulse would broaden up on propagation inside the fiber [4]. Quite often, an alternative parameter D is used to characterize the dispersion instead of β_2 and is expressed in units of ps/nm/km. D is related to $\beta_1$and β_2 by

$$D = \frac{d}{d\lambda}\left(\frac{1}{v_g}\right) = \frac{d\beta_1}{d\lambda} = -\frac{2\pi c}{\lambda^2}\beta_2 \quad . \tag{3.5}$$

The wavelength at which β_2 and D become zero is known as zero-dispersion wavelength and is denoted by λ_0. Figure 3.1 shows the dependence of β_2 on wavelength for bulk silica glass. As seen in Fig. 3.1, β_2 vanishes at a wavelength of about 1.27 μm and becomes negative for longer wavelengths [12]. In optical fiber, the total dispersion includes both the material dispersion of bulk glass and waveguide dispersion of cylindrical dielectric waveguide. The main contribution of waveguide dispersion to β_2 is to shift λ_0 slightly toward longer wavelengths. λ_0 is approximately equal to 1.31 μm for SSMF [12]. Figure 3.2 shows the measured dependence of total dispersion parameter D on wavelength for the SSMF [12]. For $\beta_2>0$ (or $D<0$), i.e. for wavelengths such that $\lambda < \lambda_0$, the fiber is said to exhibit normal dispersion. In normal dispersion regime, low frequency components of an optical pulse travel faster than high frequency components

of the same pulse. For $\beta_2<0$ (or $D>0$, i.e. for wavelengths such that $\lambda>\lambda_0$), the fiber displays anomalous dispersion, where in the high frequency components of an optical pulse travel faster than the low frequency components.

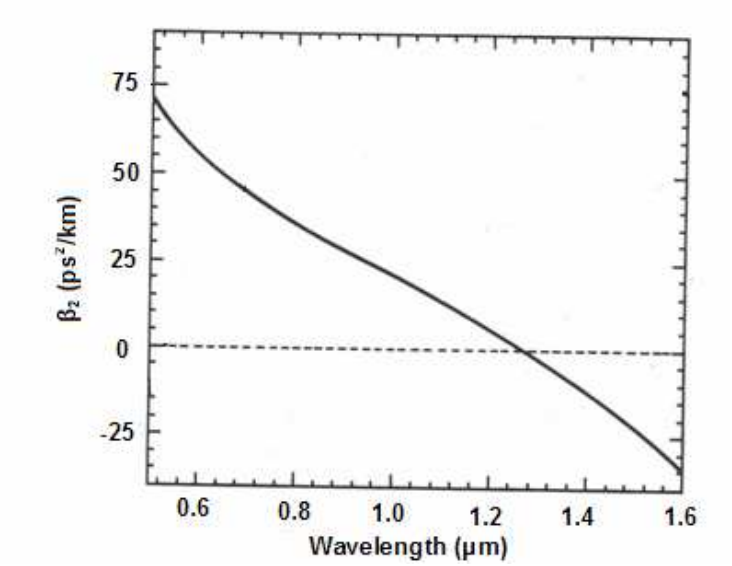

Fig. 3.1. Dependence of β_2 on wavelength for bulk silica glass. (Revised from Fig. 1.5 in Ref. [12]).

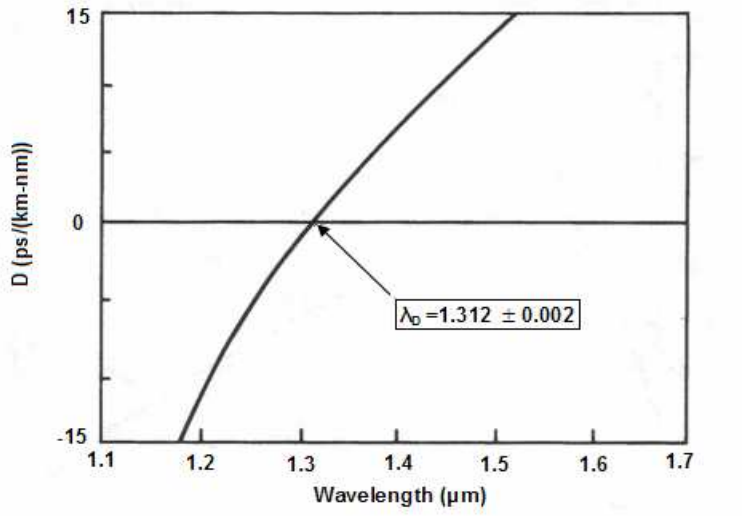

Fig. 3.2. Measured dependence of dispersion parameter *D* on wavelength for a standard single-mode fiber. (Revised from Fig. 1.6 in Ref. [12]).

3.3 Overview of Transmission Optical Fibers for WDM Systems

Since different types of optical fibers have different dispersion properties, the value of dispersion of an optical fiber becomes an important parameter of interest. An optical fiber can have small, moderate or large value of dispersion. The choice of optical fiber dispersion in modern WDM systems cannot be made without considering the detrimental nonlinear optical effects. Nonlinear effects increase with the decrease in the local dispersion of the transmission fiber. Four-wave-mixing (FWM) is a nonlinear process by which signals at different wavelengths are mixed together to produce new signals at new wavelengths. If the FWM-generated signals have same frequencies as some WDM channels, it leads to crosstalk among channels, particularly when all channels are equally spaced in frequency. In order to avoid the interchannel crosstalk, it is necessary to introduce a phase mismatch in the FWM-generation process. For systems employing optical fibers whose dispersion is small, the phase mismatch to suppress FWM can be achieved by increasing the channel spacing. However, the ultimate goal of employing WDM systems is to transmit as many channels as possible for a given available bandwidth. Hence to minimize the effects of FWM and at the same time utilize the available bandwidth, it is favorable to use fibers with large dispersion. Another nonlinear effect such as self-phase modulation (SPM) in presence of dispersion can affect the intensity profile of the signal [12]. SPM enhances the effect of dispersion, i.e. more severely broadens the pulse, when the operating wavelength is in the normal dispersion regime (D<0). On the contrary, SPM may fully or partially cancel the effect of dispersion (i.e. make the pulse narrower and its spectrum broader) in the anomalous

dispersion regime (D>0). Neither temporal nor spectral broadening is desirable in a WDM system, which limits the absolute value of dispersion that can be used with a pulse of a given peak power. Furthermore, the third nonlinear effect, the cross-phase modulation (XPM) can only be observed when dispersion is not zero, as it converts phase modulation into amplitude jitter. It can be reduced by increasing the group velocity difference between neighboring WDM channels. Thus to minimize the nonlinear effects in WDM systems, the channel separation and dispersion of the optical transmission fiber have to be properly chosen to satisfy the (sometimes conflicting) requirements on keeping the various nonlinearities under control. Here we consider three different optical transmission fibers that are commonly deployed in optical communication links.

3.3.1 Standard Single-Mode Fiber (SSMF)

SSMF, also known as Non-Dispersion Shifted Fiber (NDSF), is the most commonly deployed transmission optical fiber and is an example of a fiber having large local positive dispersion D. It has its λ_0 at 1310 nm, making it suitable for inexpensive short-range direct-modulated laser links. It can also operate at 1550 nm band, where the fiber loss has a minimum of ~ 0.19 dB/km and has a high dispersion value of 17 ps/nm/km. In this wavelength window, large dispersion in the SSMF transmission fiber results in large accumulated dispersion and hence requires dispersion compensating techniques (dispersion mapping). The high dispersion of SSMF practically eliminates FWM, but leaves XPM and SPM penalties highly dependent on the particular dispersion map used. Examples of this type of fiber are Corning SMF-28™ and OFS AllWave®.

3.3.2 Dispersion-Shifted Fiber (DSF)

By changing the refractive index profile of the core and cladding, the waveguide dispersion can be customized so that the total dispersion is zero at 1.55 μm. This type of optical fiber in which the λ_0 is shifted from 1310 nm to 1550 nm is referred to as the dispersion-shifted fiber (DSF). DSFs are optimized for operating in the 1.55 μm wavelength window. Thus, for DSF at 1.55 μm, the effect of dispersion is extremely weak, and hence dispersion compensation is not necessary. However, small dispersion implies that the nonlinear effects are no longer negligible. FWM in the DSF is very large owing to nearly perfect phase matching, which means that the channel spacing between the WDM channels has to be dramatically increased in order to suppress this degrading effect. In addition, to obtain a noticeable phase mismatch, all the channels have to be sufficiently far from the zero-dispersion wavelength. This introduces an additional constraint on the utilization of available bandwidth, further limiting the number of channels that can be transmitted. Thus with DSF, WDM operation is seriously handicapped by nonlinear effects, which has initiated the development of NZDSF.

3.3.3 Non-Zero Dispersion-Shifted Fiber (NZDSF)

Nonlinear effects in WDM systems can by reduced to a certain extent by using non-zero dispersion-shifted fiber (NZDSF). NZDSF fiber overcomes these effects by moving the zero-dispersion wavelength outside the C-band telecommunications window (1530 nm … 1560 nm). Unlike the DSF, this fiber is designed such that it has small but finite amount of chromatic dispersion at 1550 nm. This dispersion is sufficiently large to

reduce the nonlinear effects in WDM and DWDM systems. Also, since the dispersion is small, its effect is not so strong as to cause severe waveform distortion, and hence NZDSF often does not require costly dispersion-compensation techniques. There are two fiber families called NZD+ and NZD−, in which the zero-dispersion wavelength is lower and higher than 1550 nm, respectively. A typical NZD+ fiber has a chromatic dispersion of ~4.5 ps/nm/km and attenuation parameter of 0.22 dB/km at 1550 nm. The Corning LEAF™ and SMF-LS™ fibers are examples of the NZD+ and NZD− fibers, respectively.

Figure 3.3 shows dispersion versus wavelength for the fibers mentioned above.

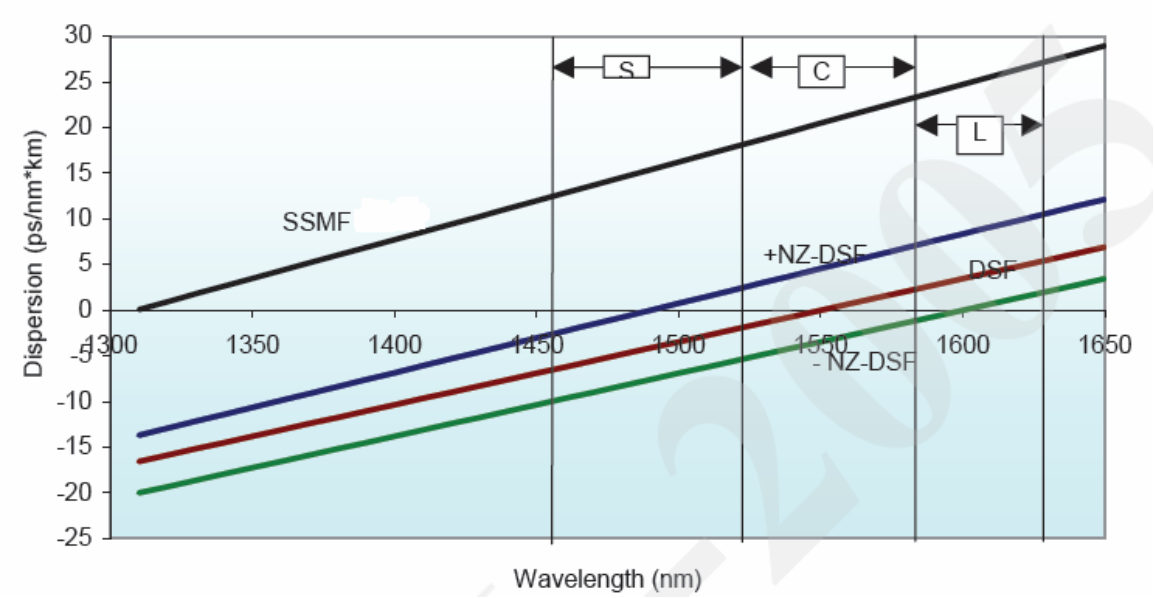

Figure 3.3 Dispersion versus wavelength for four kinds of fibers: SSMF, NZD+, NZD−, and DSF [13].

From the above discussion, we see that DSF has the lowest dispersion while SSMF has largest dispersion in the 1.55 μm wavelength window. The dispersion of NZDSF is the compromise between the DSF and SSMF. Moreover, the nonlinear effects, in general, increase with decrease in local dispersion. Hence, in order to

effectively suppress the nonlinear effects, transmission fibers with sufficiently large local dispersion have to be deployed. As stated above, SSMF fibers having large dispersion can be used to solve the problems caused by the nonlinear effects in WDM systems. However, such large dispersion results in large accumulated dispersion and hence makes dispersion compensation scheme necessary. The next section of this chapter discusses dispersion compensation using dispersion compensating fiber (DCF).

3.4 Dispersion Compensation by DCF

Dispersion compensation consists of combining fibers with different characteristics such that the average GVD of the entire link is quite low while the GVD of each fiber section is chosen to be large enough to make the FWM effects negligible and XPM effects small [7, 12]. This can be accomplished by combining two kinds of fibers, with opposite signs of β_2, so that the average dispersion is reduced to a small value.

If L_1 and L_2 are the lengths of fiber segments one and two respectively, and D_1 and D_2 their respective dispersion parameters, then the condition for 100% dispersion compensation can be given as [12]:

$$D_1L_1 + D_2L_2 = 0 \,. \tag{3.6}$$

If $L_1 = L_2$, i.e. if two segments are of equal lengths, the fibers should have opposite dispersions, i.e. $D_1 = -D_2$, in order to satisfy equation (3.6). However, to avoid extra fiber loss due to long length of the compensating fiber, a short piece of specially designed DCF with $D < -100$ ps/nm/km is typically used.

3.4.1 Dispersion-Compensating Fiber (DCF)

DCF exhibiting a large positive value of β_2 (large negative value of D) is commonly used for compensating large accumulated dispersions in SSMFs and NZDSFs. With 100 km SSMF (D~ 17 ps/nm/km) employed as the transmission fiber, 17 km of DCF (D ~ −100 ps/nm/km) is required for dispersion compensation. DCF has a much narrower core and relatively high attenuation (α=0.5 dB/km) in the 1.55 μm wavelength region. A useful index of the performance of a DCF fiber is the so-called "figure of merit" (FOM), which is defined as the dispersion of the fiber divided by the attenuation [14]. Since DCF has high attenuation of 0.5 dB/km, it is desirable for the DCF to have large dispersion value so that short length (i.e. small loss) of DCF can be sufficient to compensate for dispersion in SSMF.

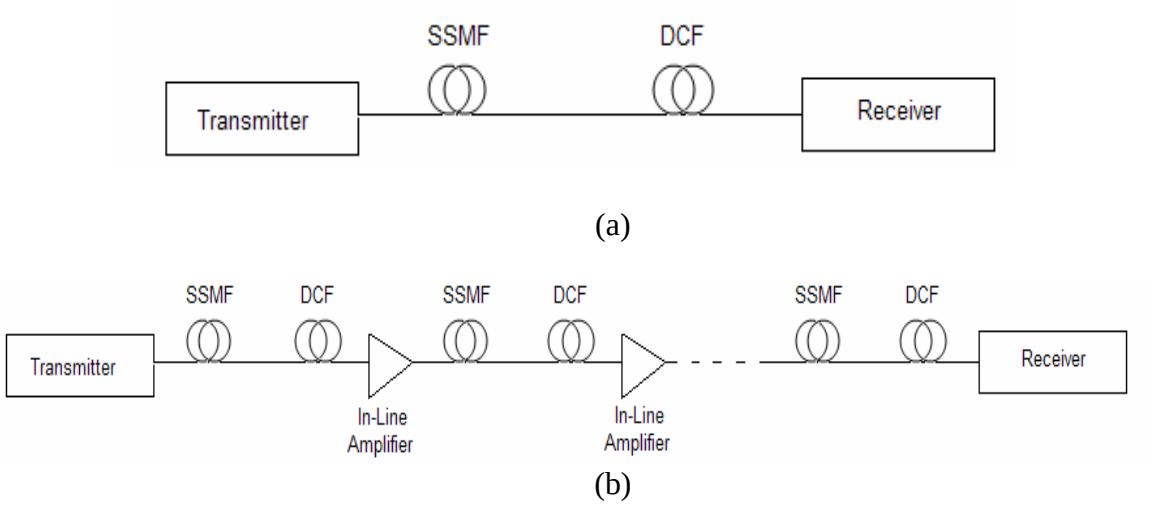

Fig. 3.4. Schematic diagram showing (a) single-span system employing DCF for dispersion compensation at the receiver, (b) multi-span system employing DCF at each inline amplifier.

In single-span systems, dispersion compensation is performed by placing the DCF near the transmitter or the receiver, as depicted in Fig. 3.4(a). However, in multi-span

systems dispersion compensation is commonly performed by placing DCF at the inline amplifier site (typically, between two stages of the amplifier) to achieve periodic dispersion compensation along the transmission link, as shown in Figure 3.4(b). This type of periodic compensation is also known as dispersion management. In advanced systems, the periodic compensation is less than 100%, and the remaining residual dispersion can be fully or partially compensated at the transmitter and the receiver sites, giving rise to various dispersion maps.

3.4.2 Splicing SSMF to DCF

As mentioned in the preceding Section, it is necessary to combine two kinds of fibers with opposite signs of β_2 to get a small average value of dispersion of the entire transmission link. This joining of two optical fibers to create a continuous path for transmission is often achieved by splicing. However, splicing two different types of fibers gives high splice loss, when compared to splicing two fibers of the same kind. This elevated splice loss is due to the mode-field diameter mismatch between the two different types of fiber. Mode-field diameter is a measure of the spot size or beam width of the light propagating in a single-mode fiber. In this section we discuss splicing SSMF to DCF using arc fusion splicer.

To obtain a highly negative dispersion, DCF uses a small core with a high refractive index, resulting in a mode-field diameter of 5 μm (A_{eff} = 20 μm^2) compared to the 10 μm mode-field diameter of SSMF (A_{eff} = 80 μm^2) at 1550 nm. This large difference in the mode-field diameters results in significant signal loss when a fusion splicing technique is used to connect DCF to SSMF. It is possible to reduce the amount

of signal loss by using another fiber with intermediate mode-field diameter between 5 and 10 μm (i.e. between SSMF and DCF). This arrangement of fibers will allow more gradual decrease in the diameter and thereby help in reducing the splice loss. This technique of introducing an intermediate fiber between two optical fibers is known as bridge splicing. The intermediate fiber used here is Corning SMF-LS^{TM}, which is a single-mode NZDSF. It has an attenuation of about 0.25 dB/km and mode-field diameter of about 8.4 μm at 1550 nm (see the SMF-LS specification sheet in the Appendix F). These characteristics of SMF-LS make it a good choice as an intermediate fiber.

Fiber fusion splicing is the most widely used permanent method for joining optical fibers. Splice losses can be minimized by careful fiber preparation and by proper fiber alignment. Preparing fiber for splicing basically involves three steps: fiber stripping, surface cleaning, and cleaving. Fiber stripping involves removing the fiber coating by techniques like mechanical stripping, thermal stripping or chemical stripping. Mechanical stripping is recommended as it is inexpensive and easy to perform. However, care must be taken to avoid damaging the fiber surface. The fiber surface has to be cleaned to remove residues that remain after fiber stripping. A clean lint-free cotton pad soaked in alcohol can be used to clean the fiber surface. Cleaving is the most important step in the splicing since it is used for proper fiber-end preparation, which is a fundamental step in achieving an acceptable fusion splice. Fiber alignment becomes extremely easy with fully automated fusion splicing equipment and involves

nothing but placing the fibers in the V-groove chucks, after which the device automatically aligns the fibers.

3.4.3 Bridge Splicing

The standard single-mode fiber and the dispersion compensating fiber utilized in the recirculating loop experimental testbed have been joined together by using Fujikura FSM-40PM Arc Fusion Splicer available in our lab. We have used bridge splicing technique to combine these two fibers, wherein SMF-LS has been employed as intermediate bridge fiber. Splicing has been conducted by carefully observing the above mentioned fiber preparation and alignment steps. Figure 3.5 depicts the final arrangement of fibers obtained after performing six splicing steps. The most important task here is the optimization of each splice.

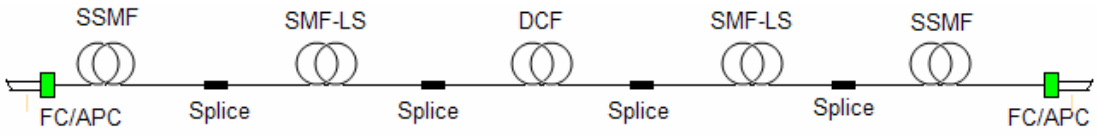

Fig. 3.5. Schematic showing the final fiber arrangement after performing six splicing steps using fusion splicer in the lab.

Light from the Tunable Laser Source (TSL) having 1550 nm wavelength and 1 mW power is launched into one end of SSMF patchcord (with FC/APC connector). Power at the output (bare-fiber) end of the patchcord (pigtail) is measured in dBm using bare-fiber-coupled power-meter. This value P1 is taken as reference for subsequent loss measurements. Figure 3.6 shows the arrangement for measuring power of optical signal at the output end of the SSMF patchcord. Once the power is measured, the SSMF end is disconnected from the power-meter and is prepared for splicing.

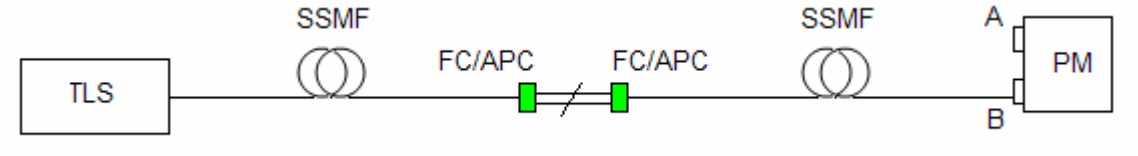

Fig. 3.6. Arrangement to measure the power of input signal by power meter (PM) before starting the splicing.

The procedure used to make and optimize four splices of the final arrangement of fibers in Fig. 3.5 is explained below in six steps.

Step 1: A temporary splice (not necessarily optimized) is made between the fiber-prepared end of SSMF patchcord and one end of DCF (e.g. 500 m spool). With the other end of DCF connected to channel B of power meter, power in dBm (P2), is measured by launching light into the SSMF FC/APC patchcord from TSL, as shown in Fig. 3.7(a). Total loss of DCF and the temporary splice is calculated by subtracting P2 from P1, i.e. Loss = (P1 – P2) dB.

Step 2: Now, the end of the DCF is disconnected from the power meter and prepared for the first splice. This prepared fiber end of DCF spool is fusion spliced with one end of 2-m-long SMF-LS fiber. The splicer settings used to perform this splice are as follows:

- Splice Mode Select: NZD – NZD
- Arc 1 time: 1500 ms
- Sweep Splice: OFF
- Taper Splice: OFF

Arc 1 time has been chosen to be 1500 ms after long and careful optimization discussed in detail in Section 3.6.

Once the splice has been made, the loss of this first splice has to be measured. This is done with the free end of SMF-LS connected to channel B of power meter and launching light at the SSMF connected to TSL by FC/APC patchcord as shown in Fig. 3.7(b). Let this power meter reading be P3 dBm. Splice loss of first-splice is then calculated by subtracting P3 from P2, i.e. Loss = (P2 – P3) dB; this value is now used as reference for the second splice.

Step 3: Once one end of the SMF-LS fiber has been spliced to DCF, the other end of SMF-LS has to be spliced to SSMF patch-cord. The splicer settings used to perform this splice are:

- Splice Mode Select: NZD – NZD
- Arc 1 time: 3000 ms
- Sweep Splice: Auto
- Sweep Time: 1500 ms
- Taper Splice: ON

Again, these settings have been selected as a result of optimization process discussed in Section 3.6.

The power of optical signal, P4 dBm, at the output end of SSMF patchcord is measured by using the fiber arrangement shown in Fig. 3.7(c) (now, with FC/APC-connected power meter). Splice loss of the second splice is then calculated by subtracting P4 from P3, i.e. Loss = (P3 – P4) dB.

Step 4: At this moment, with two splices successfully made, the temporary splice is broken, the resulting fiber arrangement is reversed as depicted in Fig. 3.7(d), and the power of signal at the output end of the DCF is measured. This power meter reading, say P5 dBm, includes the measured splice losses (first-splice + second-splice) and, in addition, the loss of the DCF fiber. As mentioned above, DCF has a loss of 0.5−0.7 dB/km, which means that 500-meter DCF spool would have 0.3−0.4 dB loss. P5 will now be used as reference for the third splice.

Step 5: Third splice is performed between the free end of DCF and one end of a second SMF-LS fiber piece, which is also 2 m long, using the same splicer settings as those mentioned in step 2. Power meter reading is noted as P6 dBm with the arrangement shown in figure 3.7(e). Third-splice Loss = (P5 – P6) dB. P6 dBm is used as reference reading to calculate the fourth-splice loss.

Step 6: Fourth splice, which is the last splice, is performed between the free end of SMF-LS fiber and one end of the second SSMF patchcord. This splice is carried out using the splicer settings of step 3. Power meter reading P7 dBm is noted as shown in Fig. 3.7(f). Fourth-splice Loss = (P6 – P7) dB. By subtracting P7 from the TSL output power P8 measured in setup of Fig. 3.7(g), the overall loss suffered by the signal propagating through the fiber link of Fig. 3.7(f) is calculated as (P8 – P7) dB. This loss includes the splice loss of all the four splices plus the losses of two SSMF patchcords (pigtails), DCF spool (e.g. 500 m) and two SMF-LS fiber pieces (each 2 m long).

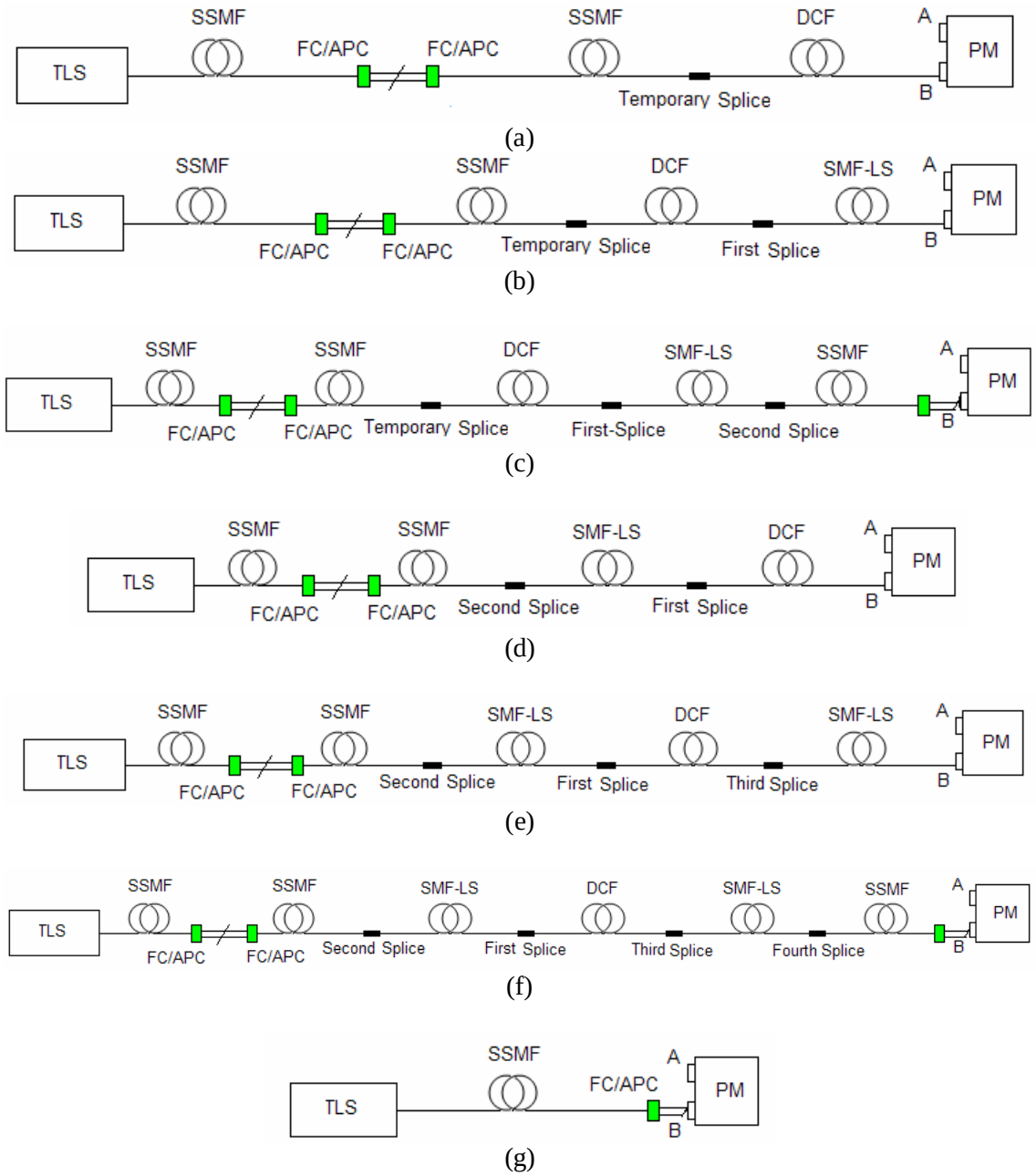

Fig. 3.7. Arrangements to measure power of output signal after (a) the temporary splice, (b) the first splice, (c) the second splice, (d) breaking the temporary splice and reversing the fiber arrangement, (e) the third splice, and (f) the fourth and final splice. The TSL output power is measured by the setup (g).

3.5 Splicing Results

Using the aforementioned six steps of bridge-splicing technique, DCF spools of lengths 500 m (two spools), 1.25 km (one spool) and 2.5 km (one spool) have been spliced to SSMF patchcords (pigtails). Splice loss less than 0.2 dB was obtained between SSMF and SMF-LS. Furthermore, splice loss less than 0.4 dB was achieved between SSMF-LS and DCF. Thus, an overall splice loss, between SSMF and DCF, was consistently accomplished in the 0.5 to 0.55 dB range. With DCF directly spliced to SSMF, splice loss $\geq$ 0.9 dB was obtained, which is considerably higher than the overall splice loss of bridge-splice technique. This proves that splice loss between SSMF and DCF can be significantly reduced by introducing SMF-LS, which can be spliced to both DCF and SSMF with low loss. The table below illustrates the total loss for fiber arrangement of figure (f) when DCF spools of lengths 500 m, 1.25 km and 2.5 km are used.

Table 3.1. DCF length and corresponding total loss.

DCF Length	Total Loss in dB
500 m	< 1.4
500 m	< 1.4
1.25 km	< 1.7
2.5 km	< 2.5

3.6 Splicing Parameters

The splice results mentioned in Table 3.1 were achieved after choosing appropriate splicing parameters, which required long and careful optimization process. The final optimized parameters set on the fusion splicer for splicing SMF-LS fiber to DCF and SSMF, respectively, were already mentioned in step 2 and step 3 of section 3.4.3. In

both cases, the splice mode selected for splicing on fusion splicer was NZD-NZD. The advice given to us by our Corning Inc.'s colleagues was to achieve a 'tuck' splice by heating DCF for only short time to avoid the collapse of refractive index profile. The main parameters that caused variations in the splice loss were Arc 1 time, sweep splice, sweep time, and taper splice. On the other hand, the parameters which hardly affected the splice loss were Arc 2 time, Arc 2 power, Arc 2 ON-Time, Arc 2 OFF-Time, and Prefuse Time. The original factory settings of important parameters of NZD-NZD mode were: Arc 1 time = 3000 ms, taper splice = OFF, and sweep splice = OFF.

The final splicer settings used to splice SMF-LS to DCF are:

- Splice Mode Select: NZD – NZD
- Arc 1 time: 1500 ms
- Sweep Splice: OFF
- Taper Splice: OFF

Splices performed with the original factory settings yielded splice loss > 1 dB and hence we had to vary the parameter Arc 1 time in 100 ms steps. Arc 1 time $\geq$ 2000 ms consistently resulted in splice loss $\geq$ 1 dB. Using taper splice and varying sweep time did not make any noticeable difference and the loss continued to remain $\geq$ 1 dB. When Arc 1 time was varied between less than 2000 ms to 1000 ms, splice loss $\geq$ 0.6 dB was achieved, but was not consistent and sometimes even produced loss $\geq$ 1 dB. Furthermore, with Arc 1 time < 1000 ms, bubbles were formed in most of the splices. With Arc 1 time set to 1500 ms, splice loss < 0.4 dB was consistently achieved.

The final splicer settings used to splice SMF-LS to SSMF are:

- Splice Mode Select: NZD – NZD
- Arc 1 time: 3000 ms
- Sweep Splice: Auto
- Sweep Time: 1500 ms
- Taper Splice: ON

With original factory settings of NZD-NZD, splice loss between 0.2 and 0.25 dB was consistently achieved. Reducing the Arc 1 time didn't make much difference in the results. With Arc 1 time of 3000 ms and taper splice ON, loss of 0.2 dB was achieved. But the splice loss was not consistent when splicing was performed with same settings repeatedly. Introducing sweep splice made considerable difference and loss < 0.2 dB was consistently achieved. However, sweep splice had to be operated in auto-mode as the other options L (left sweep), R (right sweep), and L-R (left and right sweep) did not help in reducing the loss below 0.2 dB. Sweep time was set to maximum (default setting, i.e. 1500 ms), as changing it did not make any difference.

CHAPTER 4

RECIRCULATING LOOP TESTBED

4.1 Introduction

Modern optical fiber communication systems employ hundreds of components and thousands of kilometers of optical fiber. In the lab environment, the cost and space considerations do not permit us to employ so many components and more than several fiber spans. The recirculating loop enables characterization of long-haul systems by putting a few components and a limited length of fiber in a loop and letting the signal propagate through them many times. In addition to helping in testing various lumped devices, it also facilitates studying the degrading effects of dispersion, noise and optical nonlinearities in ultra-long-haul transmission systems and networks. This chapter describes in detail the experimental setup and operation of our recirculating loop. The basic principles and operation of the loop are similar to those employed in telecom industry [15, 16].

4.2 Experimental Setup

Figure 4.1 shows the schematic diagram of the recirculating loop setup built in our lab. Entire testbed is contained in two movable racks as depicted in Fig. 4.2. The recirculating loop consists of four basic elements: transmitter, loop switch controller, transmission link, and receiver.

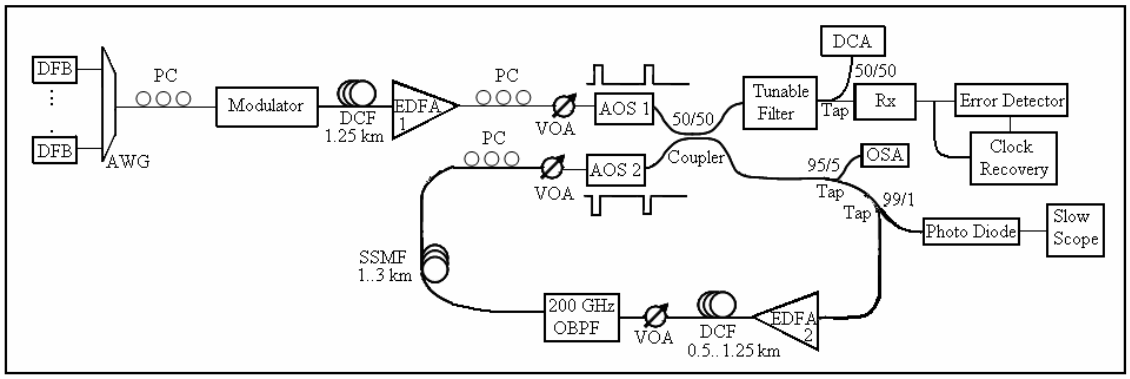

Fig. 4.1. Experimental setup of recirculating loop. PC−polarization controller, OBPF−optical bandpass filter.

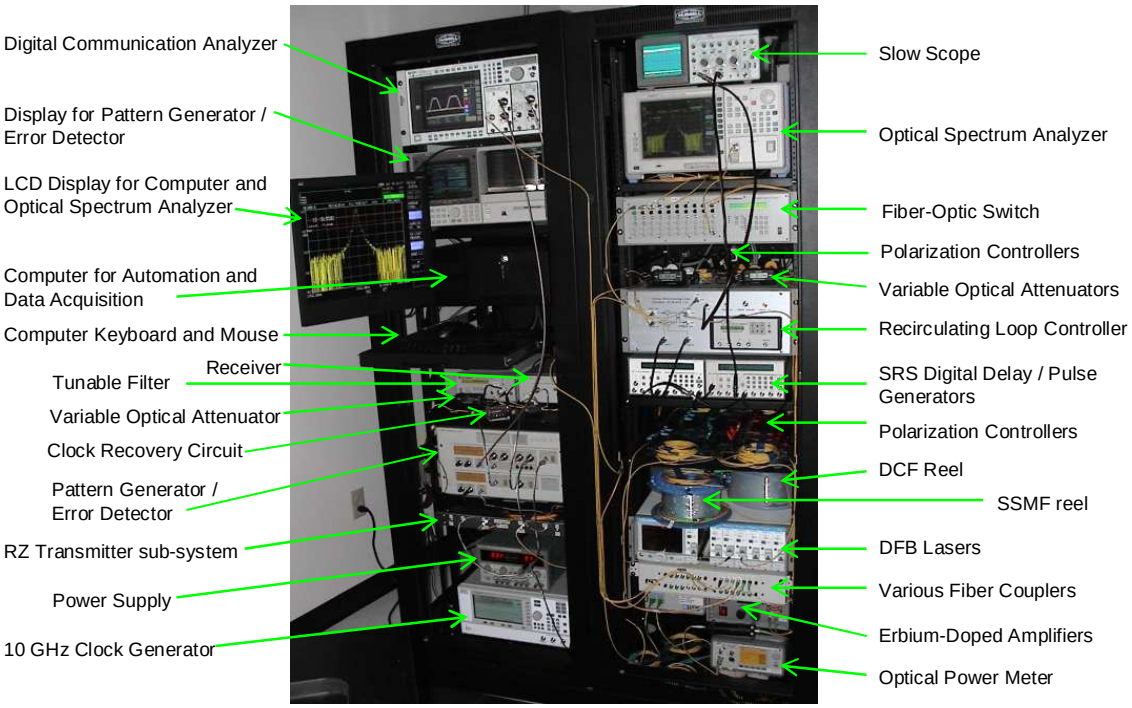

Fig. 4.2. Recirculating loop testbed configured in two movable racks.

1. *Transmitter* contains 36 distributed feedback (DFB) lasers, arrayed-waveguide grating (AWG) multiplexer as a passive combiner, polarization controller (PC), modulator, and an erbium-doped amplifier (EDFA). 36 DFB lasers separated by 100 GHz are multiplexed with an AWG and modulated using a 10 Gb/s electro-

optic modulator described in Section 2.7. DFB lasers are used for their very narrow linewidth, and low relative intensity noise. External modulator used here is a $LiNbO_3$ Interferometric Mach-Zehnder Modulator (MZM) which imposes the same data stream generated by pattern generator onto 36 DFB lasers. We de-correlate the patterns of these 36 WDM channels by sending the signals through 1.25 km of DCF (−150 ps/nm). To compensate for the losses of modulator, controller, multiplexer, and DCF we use an EDFA.

2. *Loop Switch Controller* is the most important active component in a recirculating loop which injects and circulates the bit stream. It is comprised of the following main parts: two acousto-optic switches (AOSs), one 3-dB coupler, 1% and 5% taps, two polarization controllers, and two variable optical attenuators (VOAs). The signal is coupled into the loop by means of a four-port (2×2) optical 3-dB coupler. In a 3-dB coupler, light enters a particular port on one side and exits from each of the two ports on the other side. Thus the signal is split in half. The AOSs are the essential elements in the loop switch and work in counter-phase, i.e. when AOS 1 is in “on” state (i.e. transparent) to load the loop, AOS 2 is in the “off” state (no light propagates through it), and vice versa.

   When AOS 1 is open (“on” state), signal comes from it into the 3-dB coupler, from which half of the signal goes to the receiver and the other half goes into the recirculating loop. By the time the signal reaches the end of the loop, AOS 1 closes (“off” state), AOS 2 opens, and the signal circulates in the loop for as long as AOS 2 is open. The variable optical attenuator is used to

balance gain and loss after each round-trip so that the total signal powers after each round-trip are the same. This balance operation eliminates the wild transients of EDFAs that can damage the optical components in the loop. Even though the AOSs are designed to be polarization-insensitive, they still exhibit some polarization-dependent loss (about 0.2 dB). To prevent accumulation of this loss over many circulations, we employ polarization controllers inside and outside the loop. The receiver equipment is triggered to take data after the desired number of circulations. Two SRS (Stanford Research System Inc.) DG535 Digital Delay/ Pulse Generators are used to trigger the AOMs as well as the receiver equipment. The length of the burst generated by the first pulse generator corresponds to the loop length, in order to fill it up completely. The duty cycle is adjusted in such a way to allow the burst to recirculate in the loop as many times as necessary for the investigation.

A 5% tap (95/5 coupler) is used in the loop switch to monitor the signal spectrum at any given circulation on an Optical Spectrum Analyzer (OSA). A tap is a coupler that splits only a small part of the light into one (tap) port leaving the rest in the other (through) port. Hence 5% of the signal goes to OSA and the remaining 95% goes into the loop. In addition, a 1% tap is connected to photodiode to monitor the power inside the loop.

3. *Transmission Line* basically contains variety of components inside the loop, including device under test (DUT) or fiber under test (FUT). As depicted in the Fig. 4.1, the transmission link of our loop contains one high-power erbium-

doped fiber amplifier EDFA 2, optical bandpass filter, 0.5…1.25 km of Corning DCF, and 1…3 km of SSMF (Corning SMF-28e^{TM}). DCF is used to compensate the accumulated dispersion due to SSMF fiber in the loop. EDFA 2 is placed at the beginning of the loop to boost the signal before launching it into the transmission line. An EDFA can also be placed after the DCF spool in the link to compensate for the DCF losses as DCF has high attenuation. AWG demultiplexer is used as a 200-GHz-wide optical bandpass filter (OBPF). It is only used with single-channel signal to prevent accumulation of out-of-band ASE (Amplified Spontaneous Emission) noise in the loop. Furthermore, an optical isolator should be placed between EDFA and the filter to prevent propagation of back reflection generated by the filter. Here we use an EDFA with internal optical isolator. During the operation of loop, loss and gain need to be balanced so that there is constant unity loop gain. This is achieved either by adjusting the loop gain using EDFA 2 pump current or by changing the loop loss using VOA.

4. *Receiver* continuously receives data from every circulation from the 3-dB coupler. The error detector connected to the receiver operates in the burst mode gated by the digital delay / pulse generator in order to detect the errors occurring after a particular number of circulations. The error detector compares the bits during the gate window with the bits supplied to the transmitter by the pattern generator. Any difference between the patterns represents the bit error. The device used in our testbed for error detection is Error Performance Analyzer,

model number 70843B by Agilent. A 0.22-nm-wide tunable filter used at the input of the receiver acts as a demultiplexer and selects specific channel to be measured by 10 Gb/s receiver. In future 2R regeneration experiments, this filter will also perform off-center filtering.

4.3 Triggering Setup

As mentioned above, two SRS digital delay/pulse generators, termed DG 1 and DG 2 are used to trigger AOSs, receiver, Optical Spectrum Analyzer (OSA) and the Digital Communications Analyzer (DCA) simultaneously. Figure 4.3 shows trigger connections between these devices. Both generators have five delay output ports: T0 (internal trigger), A, B, C, D and four pulse outputs AB, −AB (i.e. inverted AB), CD, and −CD. DG 1 controls AOS 1 and AOS 2, as well as the error detector and DCA. DG 2 is externally triggered by −CD output on DG 1 and controls diagnostic devices: OSA and slow oscilloscope.

The +AB output on DG 1 is connected to the AOS 1 driver which drives AOS 1. Since the pulse that drives AOS 2 is the complementary to the pulse that drives AOS 1, AOS2 driver is connected to −AB (i.e. inverted) output on DG1.

The measurement window corresponding in time to a particular circulation is selected by gating the DCA (fast oscilloscope), error detector, and OSA. The Agilent DCA specifies gating width of 1 μs at 10 GHz. The gating pulse input at least 1 μs long is supplied by DG 1 using the CD output. The same signal is also used to gate the error detector. Despite having option 100 (enhanced trigger), our DCA has shown very poor time-jitter

performance in gated trigger mode. Therefore, in the future we plan to use another AOS to gate the input signal to the DCA which will be continuously triggered.

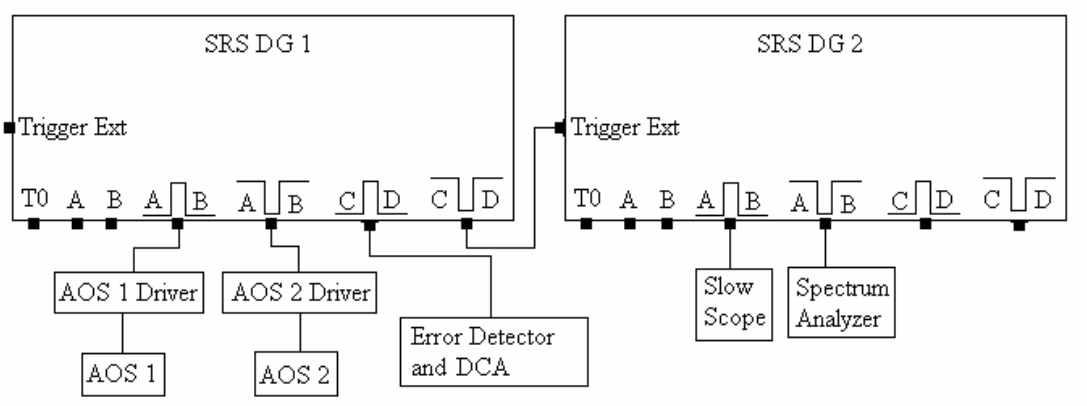

Fig. 4.3. Schematic showing connections between SRS delay / pulse generators 1 and 2 to other equipment of the setup.

Gating input of the OSA (EXT TRIG IN) needs a negative-logic TTL signal, hence −AB on DG 2 is used trigger it. The OSA gating pulse must be at least 5 μs long. In addition, OSA essentially integrates the signal over 120 μs preceding the gate. Thus, to show the true spectrum after a particular circulation, either long loop length (propagation time longer than 120 μs) is needed, or the OSA input needs to be optically gated using another AOS.

High-Z termination needs to be set on DG 1 and DG 2 for all TTL signals. In case of connection to a 50-Ohm load, the signal may decrease in amplitude, but will not change its temporal profile. On the other hand, using 50-Ohm setting on DG 1 and DG 2 would only work with 50-Ohm load and will produce a dramatically distorted waveform if connected to a high-impedance device.

4.3.1 Trigger Settings

The trigger settings are calculated similar to [15, 16]. When AOS 1 is in "on" state, the loop is loaded with the bit stream. The time taken by the signal to travel once around the loop, known as circulation time T_{circ}, can be calculated as

$$T_{\text{circ}} = \frac{L_{\text{total}}}{c_g} \ , \tag{4.1}$$

where L_{total} is the total length of fiber in the loop (SSMF+DCF) and c_g is the group velocity of light in fiber, given by

$$c_g = \frac{c_0}{n} \ , \tag{4.2}$$

where c_0 is the speed of light in vacuum and n is the refractive index of the core.

AOS 1 should be left in the ON state for at least one complete circulation time, i.e. the time of the loading state must be equal to or more than one circulation of the loop in order to allow the loop to fully fill up and ensure that the EDFAs are saturated and in steady state. The loading-state duration can be calculated by

$$T_{\text{load}} = k \times T_{\text{circ}} \ , \tag{4.3}$$

where $k \geq 1$ is the number of times the loop is filled or loaded. In our loop, we use $k = 3$.

Once the loop has been fully loaded, AOS 1 is switched off, and AOS 2 is switched on. With AOS 2 in "on" state (i.e. transparent), light propagates in the loop for the number of times decided by the repetition rate of the pulse generator. This repetition rate is calculated by

$$R_{\text{rep}} = \frac{1}{T_{\text{load}} + \left(m \times T_{\text{circ}}\right)} \ , \tag{4.4}$$

where m is the number of times the bit stream circulates in the loop before the loop is reloaded. This calculated R_{rep} is set in the trigger menu of DG 1.

In the first demonstration of our loop's operation, we have put 1.25 km of DCF and 1 km of SSMF into the loop. In order to overcome long (120 μs) integration time of the OSA, we have added 30 km of LEAF fiber to the loop. Then L_{total} = 32.25 km. Using n=1.5 for glass, we obtain T_{circ} = 161 μs, which is close to the experimentally measured value of T_{circ} = 158 μs. With k = 3, we have T_{load} = 474 μs. The multichannel 2R regeneration experiment needs 11.2 km of DCF. Thus, with 1.25 km of DCF in the loop, the number of circulations m is set to 9. This results in a repetition rate of 527 Hz.

4.4 Recirculating Loop Results

Figure 4.4 shows the timing diagram of our recirculating loop (slow-oscilloscope trace). The two lower traces show the loading and unloading waveforms applied to AOS 1 and AOS 2, respectively. Top trace shows the signal power in the loop measured by the photodiode at 1% tap port. The narrow (~100 ns) spikes represent AOS transients between the circulations. Using loading state equal to k = 3 circulations allows us to distinguish the loading time from the subsequent circulations even in the absence of the two lower traces. One can easily see that the power stays constant from circulation to circulation, i.e. the loss and gain in the loop are balanced. Otherwise, in addition to the narrow AOS transients we would have seen longer (tens of μs) EDFA 2 transients between the circulations. The second from the top trace in Fig. 4.4 shows the timing of the measurement window (gate). It selects 8^{th} circulation to be characterized. The gate has been pushed toward the end of the circulation in order to allow for 120-μs OSA

integration time to precede the measurement. By changing delay C on DG 1, we can move the gate to any other circulation as well.

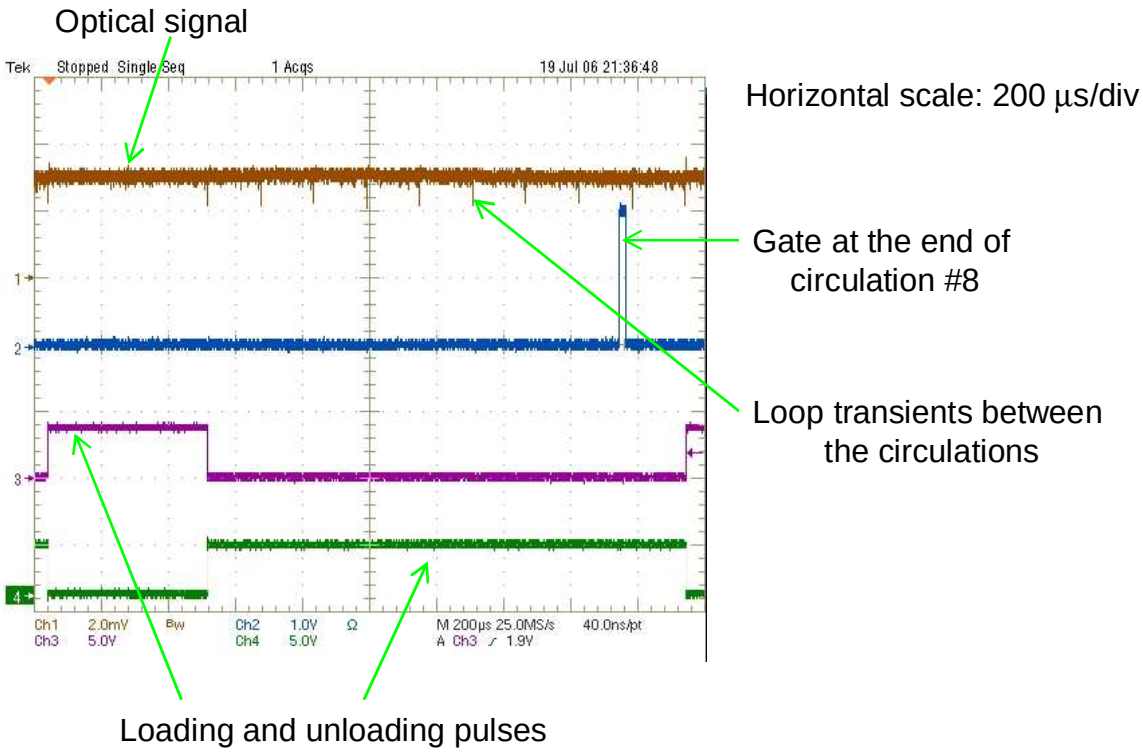

Fig. 4.4. Recirculating loop timing diagram.

Figure 4.5 shows the signal spectra after *N* circulations through the loop, when a single channel modulated by a CS-RZ format at 5 Gb/s data rate is used. From Fig. 4.5 we see that the spectrum broadens (up to ~7 times) and flattens at the top as the signal propagates, as predicted by the 2R regenerator theory [1, 17]. This broadening of the spectrum is the result of self-phase modulation (SPM) and is essential for 2R regeneration. Our results indicate that the loop is ready for 2R regeneration experiment.

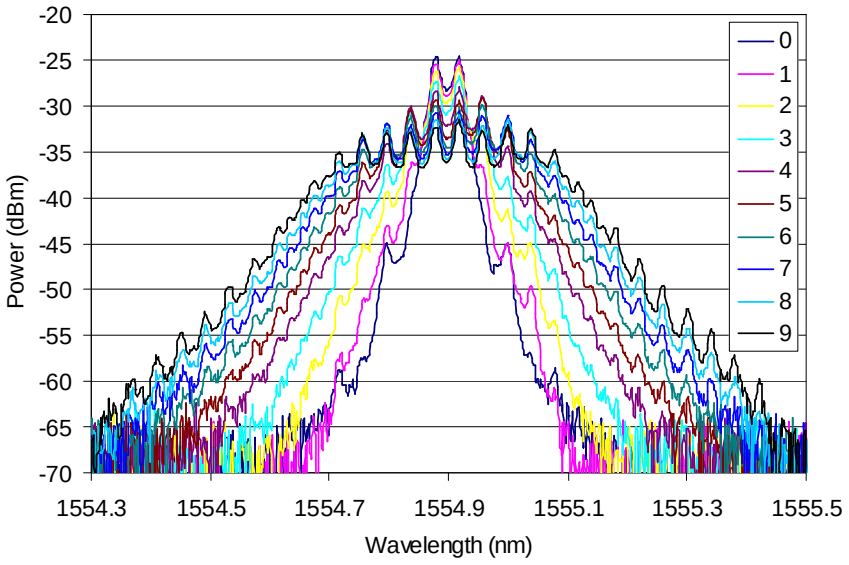

(a)

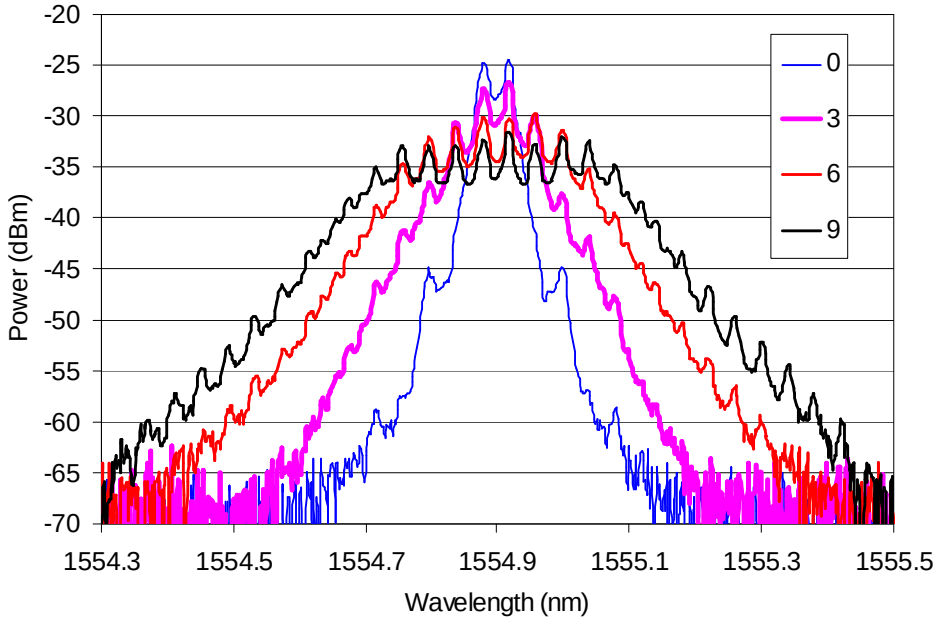

(b)

Fig. 4.5. Optical spectra for CS-RZ after N = (a) 0, 1, 2, 3, 4, 5, 6, 7, 8, 9 and (b) 0, 3, 6, 9 circulations.

CHAPTER 5

CONCLUSIONS

This thesis has focused on constructing the reciculating loop testbed intended for proof-of-principle demonstration of all-optical multichannel 2R regeneration in our lab.

We have successfully built two transmitter modules operating at bit rates up to 10 Gb/s. This work required integrating lab-built power supplies with commercially available 10 Gb/s electro-optic modulators and RF drivers, and assembling them in rack-mounted aluminum boxes. To make the device user friendly, optical and electrical connections were provided on the front and back panels of the box. The lab-built power supply section was used to provide several DC voltages necessary for the modulator operation, and helped in reducing the number of required external power supplies. This work has resulted in making two 10 Gb/s transmitter sub-systems: JDS-modulator-based RZ and Lucent-modulator-based NRZ modules. Using the JDS-modulator-based transmitter, we have successfully demonstrated generation of NRZ, RZ and CS-RZ modulation formats.

We have also successfully coupled standard single-mode fiber (SSMF) to dispersion-compensating fiber (DCF) using bridge-splicing technique. SMF-LS has been used as intermediate bridge fiber and was spliced to SSMF with loss < 0.2 dB, on one end, and to DCF with loss < 0.4 dB, on the other end. Thus, we have achieved better than 0.6 dB loss in coupling between SSMF and DCF, and obtained this result

consistently in all splices in the process of SSMF-pigtailing four DCF reels of 500 m (two), 1.25 km, and 2.5 km lengths.

After building the transmitter module and achieving good coupling between SSMF and DCF reels, we have used them along with other lab components to assemble the recirculating-loop testbed. All the components of the recirculating-loop testbed have been mounted in two movable racks and connected by optical fiber patchcords. After setting the timing of the loop switches and measurement gates and triggers, we have successfully demonstrated the loop operation with single channel. With 1.25 km of DCF as a nonlinear medium in the loop, we have observed 7-fold increase in the signal spectrum width after 9 circulations (11.25 km of DCF). This clearly indicates that the loop is ready for 2R regeneration experiments.

APPENDIX A

JDS UNIPHASE, DUAL STAGE 10 GB/S NRZ DATA MODULATOR WITH RZ PULSE GENERATOR STAGE DATA SHEET

JDS Uniphase

Final Test Data Sheet

Model Number:	10022802
Description:	Dual Stage 10 Gb/s NRZ Data Modulator with RZ Pulse Generator Stage
Serial Number:	240152C
Input Fiber Type:	Fujikura Panda SM-15-P-8/125-UV/UV-400
Output Fiber Type:	Corning SMF-28
Test Date:	11/30/2000

Performance Parameters

Parameter	Measured	Units
DC Testing		
Insertion Loss	4.5	dB
RZ Stage [illegible]	[illegible]	dB
RZ Stage [illegible]	[illegible]	V
NRZ Stage DC [illegible]	[illegible]	dB
NRZ RF [illegible]	[illegible]	V
[illegible]	[illegible]	V
FREQUENCY DOMAIN TESTING		
RZ Stage S11 (at 10.66 GHz)	-14	dB
RZ Stage Vpi (at 10.66 GHz, one-tone measurement)	8.4	V
NRZ Stage S11 (max from 130 MHz to 14 GHz)	-12	dB
NRZ Stage S21 Bandwidth (-3 dBe relative to 130 MHz)	14	GHz

NRZ RF port is AC coupled (no bias).

APPENDIX B

LUCENT TECHNOLOGIES, 40GB/S LITHIUM NIOBATE ELECTRO-OPTIC MODULATOR DATA SHEET

Product Definition Sheet
August 1999

microelectronics group

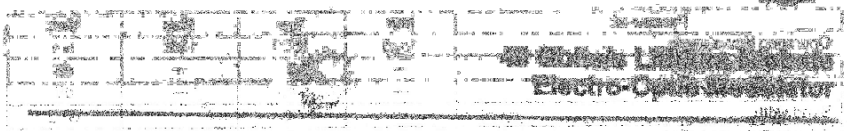

Features

- Ti-diffusion process
- Dual-drive technology
- Thin-film, 50 Ω termination in package for minimal reflections
- Low modulation voltages
- Tested to Bellcore 468
- Angled interfaces for minimal optical reflections
- Hermetic package
- Separate dc bias electrode

Benefits

- Excellent long-term bias stability over a full operational temperature range (0 °C to 70 °C)
- Adjustable chirp for long distances at high bit rates
- Internal polarizer

Applications

- Digital high-speed telecommunications
  - SONET OC-768
  - Undersea communications
- Internet data communications
- SONET test equipment

Note: This product definition sheet is intended as an aid in the process of defining a new product. The product described is available only as a model and should be used only for evaluation. This product definition sheet serves only as a basis for discussion that may or may not lead to the generation of a final specification for development. The information contained herein must not be construed as a commitment to develop, manufacture, or deliver the device described by this document. If, in fact, such a device is developed, it is likely the specification will differ, as may features and functionality.

Description

Representing the latest advancements in high-speed lithium niobate technology, the 40 Gbit/s Electro-Optic Modulator is designed for [illegible] single-mode, external amplitude modulation applications. It uses an integrated Mach-Zehnder configuration to convert single polarization CW light from a semiconductor (DFB) laser into a time-varying optical output signal. Using this source in the CW mode eliminates the need for demanding, high-speed performance from the laser and reduces its cost.

The dual-drive design inherently offers the capability to adjust the phase of the voltages on the electrodes, which produces zero-chirp modulation operation. The modulator is tested to, and meets the intent of, TR-NWT-000468.

Absolute Maximum Ratings

Stresses in excess of the absolute maximum ratings can cause permanent damage to the device. These are absolute stress ratings only. Functional operation of the device is not implied at these or any other conditions in excess of those given in the operational sections of the data sheet. Exposure to absolute maximum ratings for extended periods can adversely affect device reliability.

Parameter	Symbol	Min	Max	Unit
Storage Temperature	T_{stg}	-40	85	°C
Optical Input Power @ 1.5 µm	P_{IN}	—	30	mW
RF Voltage (RF input)	V_{RF}	—	20	V
dc Voltage (dc input)	V_{DC}	-20	20	V
Operating Temp.	T_{OP}	0	70	°C

Characteristics

Table 1. Optical/Electrical Characteristics (Tc = 25 °C)

Parameter	Min	Typ	Max	Unit
Operating Wavelength	1525	1550	1565	nm
Optical Insertion Loss	—	6	—	dB
[illegible]	—	–40	—	dB
Bandwidth	—	36	—	GHz
Drive Voltage (V_π) @ dc	—	6	—	V
Electrode Impedance	—	47	—	Ω
S11 Electrical Return Loss	—	–15	—	dB

Outline Diagram

Dimensions are in inches and (millimeters).

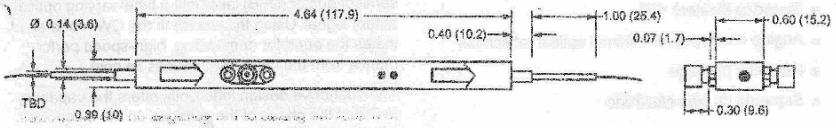

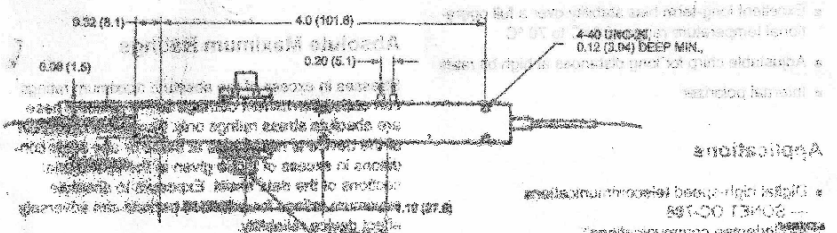

APPENDIX C

PICOSECOND PULSE LABS, MODEL 5865 12.5GB/S DRIVER AMPLIFIER DATA SHEET

MODEL 5865
12.5 GB/S
DRIVER AMPLIFIER

- **12.5 Gpbs Lithium Niobate modulator driver (8 V_{amp} output)**
- **Linear amplifier with 26 dB small signal gain and 12 GHz of bandwidth**
- **High gain with low power dissipation (2.3 watts at 8 V_{amp})**
- **Temperature compensated design for output stability**
- **Includes bias network, crossing point control & adjustable output voltage**

The Picosecond Pulse Labs Model 5865 driver amplifier is intended for use driving Lithium Niobate modulators or as a linear amplifier.

The 5865 includes internal temperature compensation for excellent output stability over temperature, and exhibits both high output and low power dissipation. It also incorporates internal sequencing circuitry, making it insensitive to power supply application sequence.

Typical 10.66 Gb/s Eye Measurements

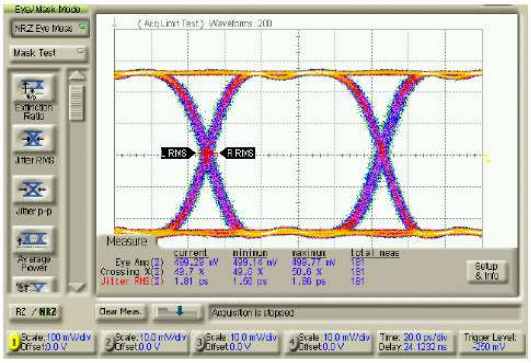

Input Test Signal [1]

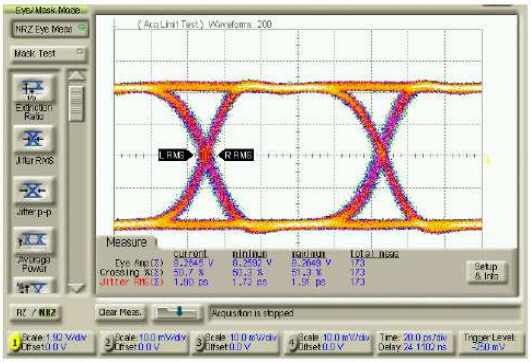

Output Response [2]

[1] Input test signal generated by Agilent Pattern Generator model 70843B.
[2] Output response measured using Agilent oscilloscope model 86100A with model 83484A 50 GHz plug-in module.

5865 Electrical Specifications

PARAMETER	SYMBOL	UNITS	MIN	TYPICAL	MAX	COMMENTS
Polarity						Non-inverting
Output Eye Voltage with V_{gc} = 0 V	V_{OUT}	V_{amp}	7.5	8.0		V_{in} = 0.5 V_{amp}, 12.5 Gb/s PRBS
Output Eye Voltage with V_{gc} = -15 V	V_{OUT}	V_{amp}		1.0	2.0	V_{in} = 0.5 V_{amp}
Upper Frequency 3 dB Point	$f_{3dB,upper}$	GHz		12		Small signal, relative to gain at 2 GHz
Lower Frequency 3 dB Point	$f_{3dB,lower}$	kHz		30		Small signal, relative to gain at 2 GHz
Small signal gain	S_{21}	dB		26.5		Measured at 2 GHz
Output Power at 1dB Gain Compression	P_{1dB}	dBm		23.5		Measured at 2 GHz
Deconvolved Rise / Fall Time [1]	$t_{r,f}$	ps		14 / 23	20 / 28	10% to 90%, V_{in} = 0.5 V_{amp}, 12.5 Gb/s PRBS
Additive Jitter [1] RMS Peak-to-Peak		 ps ps_{pp}		 0.7 4	 1.5 8	V_{in} = 0.5 V_{amp}, 12.5 Gb/s PRBS, measured at crossing point
Output Eye Voltage Variation Over Operating Temperature Range	ΔV_{OUT}	%		± 3	± 5	V_{gc} = 0 V, V_{in} = 0.5 V_{amp}, T_{CASE} = –5 to 75C, 12.5 Gb/s PRBS
Crossing Point Adjust		%	±15	±20		±5 V input at V_{co}, V_{in} = 0.5 V_{amp}
Crossing Point Variation Over Operating Temperature Range		%		±1.0	±2.0	0.5 V_{amp} Input, 12.5 Gb/s PRBS, T_{CASE} = –5 to 75°C, V_{gc} constant
Overshoot / Undershoot		%		5		12.5 Gb/s PRBS
Input / Output Return Loss 50 MHz < f < 5 GHz 5 GHz ≤ f < 12 GHz	S_{11}, S_{22}	dB		 -14 -11	 -12 -9	
Noise Figure	NF	dB		5.75	6.5	f = 1 GHz

[1] Deconvolution is done by root sum of squares. Input rise/fall times were 27 ps. Input jitter was 2.3 ps RMS / 9.8 ps pk-pk.

5865 Operating Specifications

PARAMETER	SYMBOL	UNITS	MIN	TYPICAL	MAX	COMMENTS
Maximum allowed Input		V_{amp}			1.5	Damage threshold for input
DC Voltage Supply (pos)	$+V_{DC}$	V_{DC}	8	8	8.25	275 mA typical with V_{OUT} = 8 V_{amp}
DC Voltage Supply (neg)	$-V_{DC}$	V_{DC}	-5.25	-5	-4.75	20 mA typical
Power Dissipation	P_{diss}	W		2.3	2.6	V_{OUT} = 8 V_{amp}, V_{gc} may be utilized to lower the output level and lower the power dissipated
Output Voltage Bias	V_{bias}	V_{DC}	-17		+33	2.5 kΩ resistor (DC current ≤ 3.5 mA),
Operating Temperature	T_{CASE}	°C	-5		75	Case Temperature
Storage Temperature	T_{CASE}	°C	-40		125	Case Temperature

Static sensitive device, limited 30 day warranty.

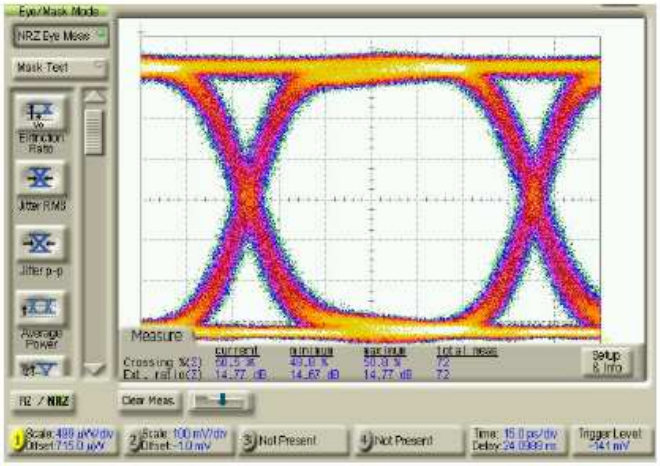

Typical Measured 10.66 Gb/s Optical Eye
(PSPL model 5865 driver, modulator controller, and OTI 12.5Gb/s $LiNbO_3$ modulator)
Input test signal generated by Advantest Pattern Generator model D3186. Output response measured using Agilent oscilloscope model 86100A with model 86109A optical plug-in module.

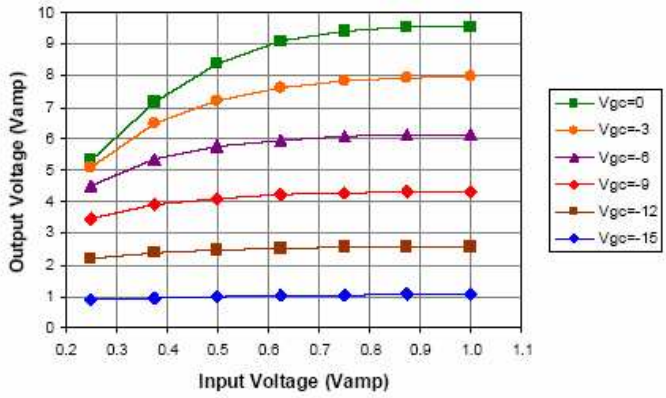

Typical Output Voltage versus Input Voltage
(Gain Control Bias = Vgc, T_{CASE} = 35C)

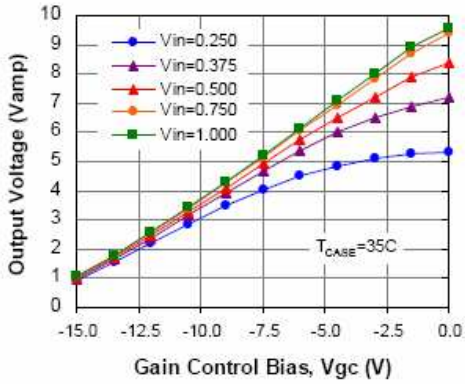

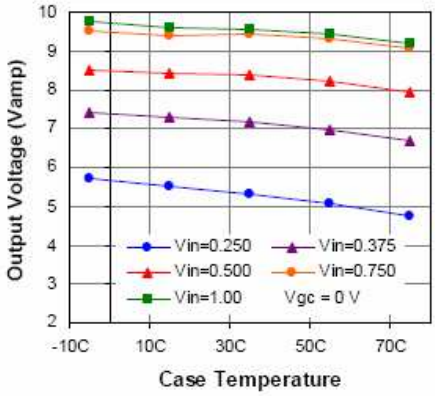

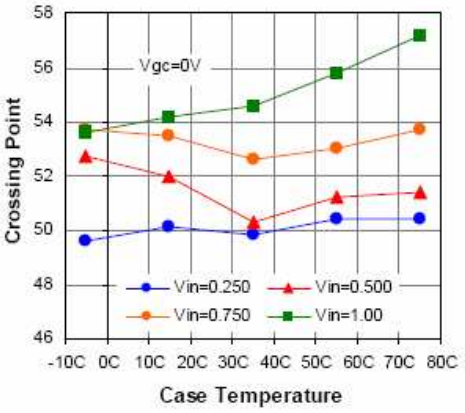

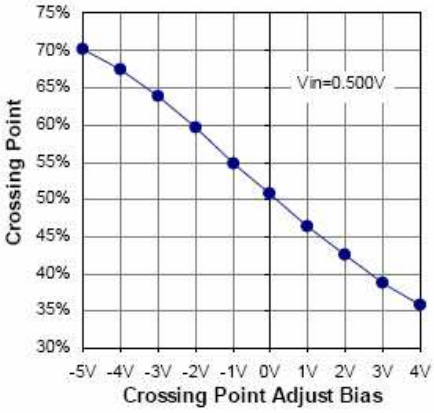

Detailed test setup information available upon request.

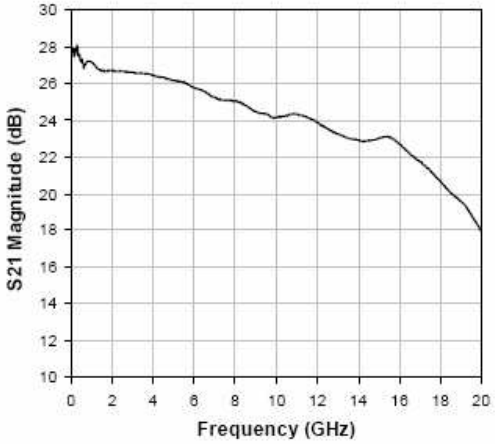

Typical Small Signal S_{21}
(measured at –20 dBm input power)

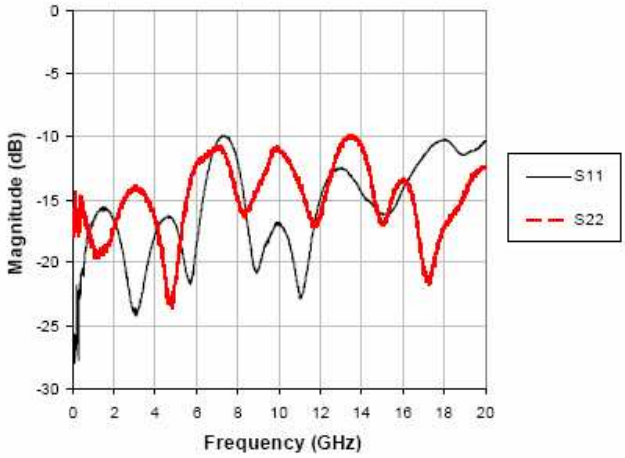

Typical Small Signal S_{11} and S_{22}
(measured at –20 dBm input power)

5865 Mechanical Dimensions (in inches unless otherwise stated)

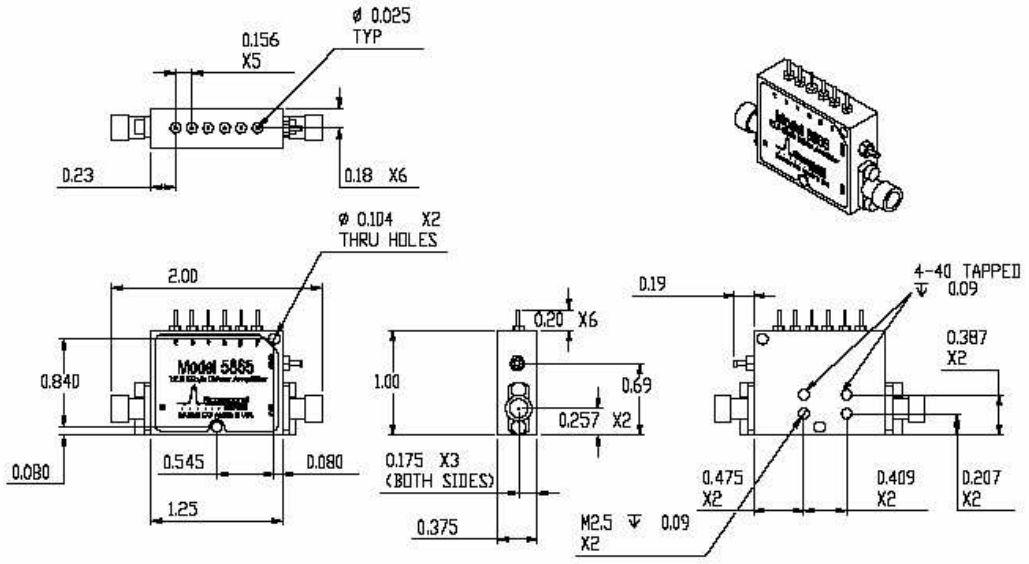

Ordering Information

Model Number	Connector Configuration *
5865-107	RF input SMA jack, RF output SMA jack, solder pins

* Other connector configurations may be available upon request.

Contact Information

Picosecond Pulse Labs
P.O. Box 44
Boulder, Colorado 80306, USA

Telephone: 1.303.443.1249
Fax: 1.303.447.2236
mailto:info@picosecond.com

Sales Support:
Telephone: 1.303.443.1249
Fax: 1.303.447.2236

Visit Us At:

www.picosecond.com

Instructions for Use

The Picosecond Pulse Labs 5865 12.5 Gb/s modulator driver may be operated using only three of the available 7 pins. The DC pins required for operation are 1, 3, and 7. The RF connectors and DC pins are diagramed and defined below.

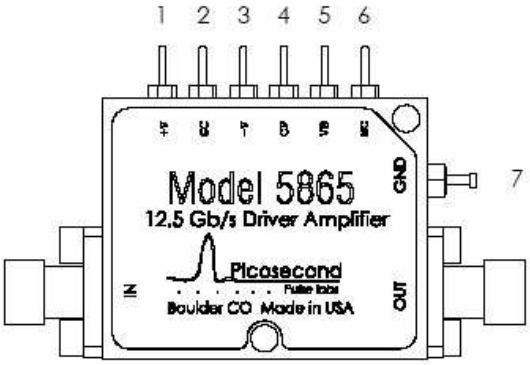

Pin Descriptions

Pin #	Pin Label	Description
	IN	SMA, signal input, $V_{amp} \leq 1.5$ V (damage threshold)
1	+V	Positive DC voltage supply, 8 V (see Note 1 and Note 2)
2	GC	V_{gc}, Variable output control, $-15\ V \leq V_{gc} \leq 0\ V$ (see Note 3)
3	-V	Negative DC voltage supply, $-5.25\ V \leq V \leq -4.75\ V$ (see Note 2)
4	CP	Crossing point adjust, $-5\ V \leq V_{cp} \leq 5\ V$ (see Note 4)
5	VB	DC Voltage bias, $-17 \leq VB \leq +33$ (see Note 5)
6	NC	No connection / Not used
7	GND	Ground connection
	OUT	SMA, signal output

Warning: The 5865 requires a ground connection at pin #7 prior to voltage application to prevent damage.

NOTES:

Note 1: At 8V, approximately 2.3W is dissipated.
Note 2: No power sequencing is necessary. Voltages may be applied in any order after ground is applied.
Note 3: Output Control: With V_{gc} at 0V, or left floating (disconnected), the driver will provide maximum gain and maximum output voltage. The user may decrease V_{gc} to decrease the RF signal gain when the driver is operating in the linear regime, or to reduce the output voltage level when the driver is operated in saturation (this will also reduce the power dissipated).
Note 4: The crossing point may vary until unit achieves thermal equilibrium.
Note 5: Voltage Bias: The VB pin allows the user to apply a *low current* (less than 3.5 mA) DC offset to the Signal Output for biasing electro-optic modulators through a 2 kΩ resistor.

APPENDIX D

JDS UNIPHASE, 10 GB/S OPTICAL MODULATOR DRIVER H301 SERIES DATA SHEET

JDS Uniphase

Discontinued Product

10 Gb/s Optical Modulator Driver

H301 Series

The H301 optical modulator driver provides a high-quality, single-ended voltage to drive an external laser modulator. Typical applications include driving EML, EAM, and Mach-Zehnder style modulators. It amplifies 2.488 to 12.2 Gb/s data input signals to >7.0 V_{P-P} drive levels. The flat gain and flat group delay response yield a high-quality, low-jitter electrical drive signal. The driver meets applicable SONET and SDH standards for OC-192 10 Gb/s optical transmitters and includes reference and detector outputs to enable external temperature-compensated control of output drive levels. The module has field replaceable input and output K-connectors for the input/output drive signals and an eight-pin connector for the detector, reference, and power interfaces.

Key Features

- Low power, 4.9 W
- Low jitter
- Data rates from 2.488 to 12.2 Gb/s

Applications

- SONET/SDH equipment
- SR, IR, LR optical transmitters

Block Diagram

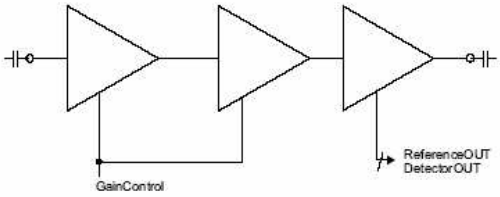

Gain and Return Loss vs. Frequency

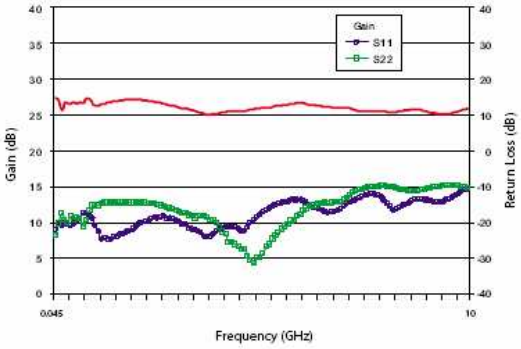

Eye Diagram

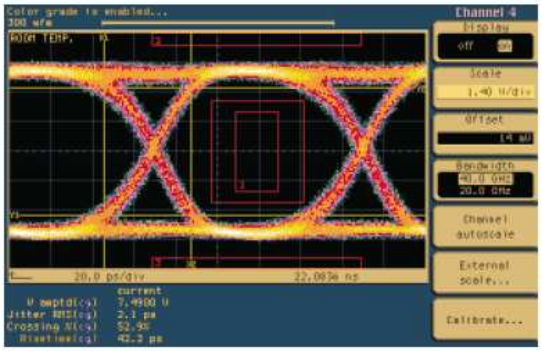

Specifications

Parameter		
Data rate		2.488 to 12.2 Gb/s
Frequency response		75 KHz to 10 GHz
Output amplitude (>7 V)	Typical	7.0 V_{P-P}
	Maximum	7.5 V_{P-P}
P_{1dB} output	Typical	>22 dBm
	Maximum	23 dBm
P_{sat} output	Typical	>24 dBm
Gain		14 to 26 dB, variable
Gain ripple		±1.5 dB
Gain control range (-10 to 0 V DC using external 510 W resistor)	Typical	12 dB
	Minimum	10 dB
Group delay (2 to 10 GHz)	Typical	±25 ps
Noise figure		11 dB
Input, output impedance		50 Ω
Input range		500 mV to 1.5 V
Input VSWR		
75 to 200 KHz	Typical	1.9
	Maximum	2.25:1
200 KHz to -10 GHz	Typical	1.6:1
	Maximum	2.25:1
Output VSWR	Typical	2.0:1
	Maximum	3.0:1
Isolated run of ones or zeros		100 bits
Pulse response	Typical	Overshoot/undershoot 10%, drop 10%, rise time 40 ps
Operating temperature		0 to 70 °C
Storage temperature		-40 to 100 °C
Operating humidity, non-condensing	Maximum	85%
Storage humidity, non-condensing	Maximum	97%
Altitude		0 to 3,048 m (0 to 10,000 ft)
Soldering process temperature (30 seconds)	Maximum	215 °C
Process temperature (24 hours)	Maximum	150 °C
Dimensions (W x H x D)		1.2 x 0.5 x 1.0 in
Power requirements		
8.0 V DC minimum	Typical	600 mA
-5.0 V DC minimum	Typical	22 mA
Total power dissipation	Minimum	4.9 W
Input/output		2.9 mm (field replacement "K")
Power detector/reference/ground		8-pin package

Package Dimensions (in inches [mm])

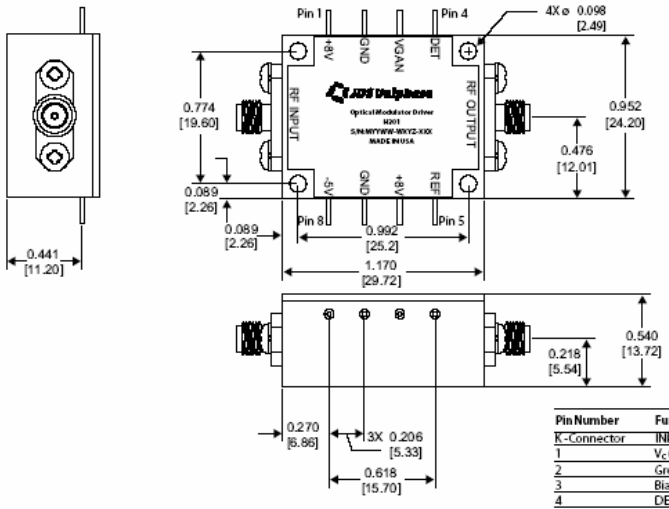

Pin Number	Function
K-Connector	INPUT (AC coupled)
1	V_C (8 V)
2	Ground
3	Bias (V_{GAIN})
4	DET (V_{DET})
K-Connector	OUTPUT (AC coupled)
5	REF
6	V_C (8 V)
7	Ground
8	V_{EE} (-5.0 V DC)
	Case is grounded internally

Ordering Information

For more information on this or other products and their availability, please contact your local JDS Uniphase account manager or JDS Uniphase directly at 800-871-8537 in North America and 1-800-8735-5378 worldwide or via e-mail at jdsu.sales@jdsu.com.

Sample: H301-1110

H301-☐☐10

Code	Connector
1	Female in, Female out
2	Female in, Male out
3	Male in, Male out
4	Male in, Female out

Code	Driver Option
1	Standard
2	Optimized for JDS Uniphase modulator
3	AM modulation input pin

JDS Uniphase

North America toll-free: 800-871-8537
Worldwide toll-free: 1-800-8735-5378
www.jdsu.com

10127929 Rev. 001 12/01

APPENDIX E

PICOSECOND PULSE LABS, MODEL 5575 BIAS TEE DATA SHEET

Picosecond Pulse Labs

Model 5575A
Bias Tee

The Model 5575A is a broadband coaxial bias insertion tee and DC blocking capacitor designed to pass fast rise pulses with minimum waveform distortion. The risetime is 30 ps with a -3 dB bandwidth extending from 10 kHz to 12 GHz. The 5575A will safely carry 500 mA of DC current. However, core saturation limits the low frequency response at DC currents above 20 mA. See Notes [1-3].

Risetime (10%-90%) **[2]**	30 ps, 35 ps max.	**DC Voltage**	50 V max.
Bandwidth (-3 dB) **[3]**	12 GHz, 10 GHz min.	**Inductance**	8 mH, ± 30%
Low Frequency (-3 dB)	10 kHz	**Core Saturation:** **Current** **< 20 mA** **100 mA** **500 mA**	 -3dB low freq. < 10 kHz 70 kHz 300 kHz
Insertion Loss (0.01 – 3 GHz)	0.6 dB, ± 0.5 dB	**DC Resistance**	0.6 O
Impedance	50 O	**CW RF Power**	3.5 W max.
Refl. Coefficient (35 ps TDR) (AC Port)	±5%, t < 100 ps, -6%, t > 100 ps	**Connectors**	SMA jacks (f)
DC Current	500 mA max.	**Capacitance**	0.22 µF, -50%, +80%
Isolation (AC – DC)	> 30 dB	**Dimensions**	1.95" x 0.5" x 1.82" (5 x 1.3 x 4.6 cm)
Return Loss [3] (AC Port)	0.1 < f < 10 GHz RL > 18 dB - 1.2 dB/GHz * f (GHz)	**Warranty**	One year. See Terms and Conditions of Sale for details

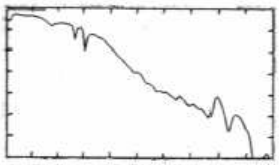

1 dB/div and 2 GHz/div
Insertion Loss

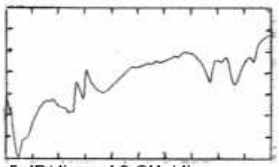

5 dB/div and 2 GHz/div
Return Loss

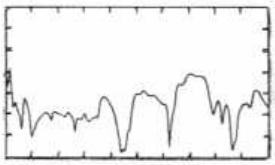

10 dB/div and 2 GHz/div
Isolation (AC-DC)

Ordering Information

Model Number
5575A-104

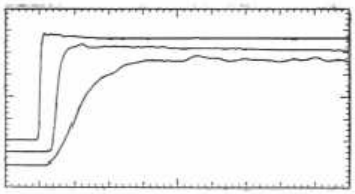

20%/div. Top to bottom: 500 ps/div, 100 ps/div, and 20 ps/div
10 ps Step Response

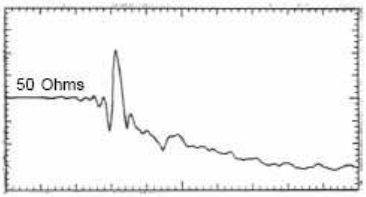

2.5% rho/div and 200 ps/div
35 ps TDR of AC port

Notes
[1] Parameters listed are typical values. They are guaranteed only when maximum and / or minimum limits are given.
[2] 10 ps risetime step response and TDR waveform measured using a PSPL Model 4015B pulse generator and an HP-54124A, 50 GHz, 9.4 ps digital sampling oscilloscope.
[3] Frequency response measured using a Wiltron 5447A, 10 MHz - 20 GHz network analyzer.

PICOSECOND PULSE LABS P.O. Box 44 BOULDER, CO 80306, USA TEL: 1.303.443.1249 FAX: 1.303.447.2236
WWW.PICOSECOND.COM

APPENDIX F

CORNING INC, SMF-LS ™ CPC6 SINGLE-MODE NON-ZERO DISPERSION-SHIFTED OPTICAL FIBER SPECIFICATION SHEET

CORNING Corning Incorporated
Telecommunications Products Division
Corning, N.Y. 14831
Tel: (910) 395-7659 (in North America)
Fax: (910) 395-7286 (in North America)
Tel: (607) 974-5354 (outside of North America)
Fax: (607) 974-7041 (outside of North America)

Corning® Optical Fiber

Product Information

PI1050

Issued: 9/98
Supersedes: 4/97
ISO 9001 Registered

Corning® SMF-LS™ CPC6 Single-Mode Non-Zero Dispersion-Shifted Optical Fiber

GENERAL

Corning® SMF-LS™ single-mode fiber is designed for use in both single and multiple channel systems operating in the 1550 nm window. This product has been developed to meet emerging 1550 nm network design requirements, including the use of erbium-doped fiber amplifiers (EDFAs) and multiple-channel "dense WDM" technology. The fiber is optimized to handle multiple high-bit-rate wavelength channels in the 1550 nm window over long system lengths. Other uses include medium to long-distance, single- and multi-channel 1550 nm systems for interoffice and long-distance applications.

SMF-LS fiber is optimized for use in the 1550 nm wavelength region. With low dispersion in this operating window, fiber information-carrying capacity is at its highest. The patented segmented core design provides low dispersion, attenuation, and bend loss at the 1550 nm operating wavelength. In addition, non-linear effects such as four-wave mixing, which might otherwise limit multiple channel operation at 1550 nm, are suppressed by ensuring non-zero dispersion across the 1530-1560 nm operating band.

Corning fiber is protected for long-term performance and reliability by CPC6 coating. Corning's enhanced dual acrylate CPC6 coating provides excellent fiber protection and is easy to work with. CPC6 can be mechanically stripped and has an outside diameter of 245 µm. CPC6 is optimized for use in many single- and multi-fiber cable designs.

SMF-LS fiber is manufactured using the Outside Vapor Deposition (OVD) process, which produces a totally synthetic, ultra-pure fiber. As a result, Corning SMF-LS fiber has consistent geometric properties, high strength and low attenuation. Corning SMF-LS fiber can be counted on to deliver excellent performance and high reliability, reel after reel. Measurement methods comply with ITU recommendations G.650, IEC 60793-1 and Bellcore GR-20-CORE.

FEATURES & BENEFITS

- Designed for use in multi-channel high-bit-rate applications.
- Patented segmented core design provides low dispersion, attenuation, and bend loss at 1550 nm.
- Outstanding geometrical properties for low splice loss and high splice yields.
- OVD manufacturing reliability and product consistency.

OPTICAL SPECIFICATIONS

- **Attenuation**

Attenuation Cell:

≤0.25 dB/km at 1550 nm
≤0.50 dB/km at 1310 nm

Point Discontinuity:

No point discontinuity greater than 0.10 dB at 1550 nm.

Attenuation at the Water Peak:

The attenuation at 1383 ±3 nm shall not exceed 2.0 dB/km.

Attenuation vs Wavelength

Range (nm)	Ref. λ (nm)	Max Increase α (dB/km)
1525 - 1575	1550	0.05

◀ The attenuation in a given wavelength range does not exceed the attenuation of the reference wavelength (λ) by more than the value α.

OPTICAL SPECIFICATIONS, (continued)

Attenuation With Bending			
Mandrel Diameter (mm)	Number of Turns	Wavelength (nm)	Induced Attenuation (dB)
32	1	1550	• 0.50
75	100	1550	• 0.05

◀ The induced attenuation due to fiber wrapped around a mandrel of a specified diameter.

Cable Cutoff Wavelength

λ_{ccf} < 1260 nm

Mode Field Diameter

8.40 ≥ 0.50 nm at 1550 nm

Chromatic Dispersion

Total Dispersion: -3.5 to -0.1 ps/(nm•km) over the range 1530 to 1560 nm

Fiber Polarization Mode Dispersion (PMD)	
	Value (ps/√km)
PMD Link Value	0.08*
Maximum Individual Fiber	0.2

*Complies with IEC SC 86A/WG1, Method 1, September 1997

◀ The PMD link value is a term used to describe the PMD of concatenated lengths of fiber (also known as the link quadrature average). This value is used to determine a statistical upper limit for system PMD performance.

PMD values may change when fiber is cabled. Corning's fiber specification supports emerging network design requirements for high data rate systems operating at 10 Gbps (TDM) rates and higher.

Dispersion Calculation
$\text{Dispersion} = D(\lambda) = \left(\frac{D(1560\text{ nm}) - D(1530\text{ nm})}{30} * (\lambda - 1560) \right) + D(1560\text{ nm})$ λ = Operating Wavelength

FOWMSPONFOUBMTQFDJGJDBUJPOT

Environmental Test Condition	Induced Attenuation (dB/km)
	1550 nm
Temperature Dependence -60≤C to +85≤C*	• 0.05
Temperature-Humidity Cycling -10≤C to +85≤C* and 4% to 98% RH	• 0.05
Water Immersion, 23≤C	• 0.05
Heat Aging, 85≤C	• 0.05

*Reference temperature = +23≤C

Operating Temperature Range

-60≤C to +85≤C

P11050

EJNFOTJPOBM TQFDJGJDBUJPOT

Tuboebse!Mfohui!)ln*;fm 4.4 - 25.2*

**Longer spliced lengths available at a premium.*

Hmbtt!Hfpnfusz

Fiber Curl: µ2.0 m radius of curvature

Cladding Diameter: 125.0 ≥ 1.0 nm

Core-Clad Concentricity: • 0.8 nm

Cladding Non-Circularity: • 1.0%

Defined as: $\left[1 - \frac{\text{Min. Cladding Diameter}}{\text{Max. Cladding Diameter}}\right] \times 100$

Dpbujoh!Hfpnfusz

Coating Diameter: 245 ≥5 nm

Coating-Cladding Concentricity: < 12 nm

NFDIBOJDBM TQFDJGJDBUJPOT

QsppgUftu

The entire length of fiber is subjected to a tensile proof stress µ 100 kpsi (0.7 GN/m^2)*.

**Higher proof test available at a premium.*

QFSGPSNBODF!DIBSBDUFSJ[BUJPOT

Characterized parameters are typical values.

Ovnfsjdbm!Bqfsuvsf;

0.16

NA was measured at the one percent power angle of a one-dimensional far-field scan at 1550 nm.

Npef!Gjfme!Ejbnfufs!bu!2421!on;

6.6 nm

UzqjdbmEjtqfstjpo;

-2.9 at 1530 nm

-0.7 at 1560 nm

Fggfdujwf!Hspvq!Joefy!pg!Sfgsbdujpo!)O$_{fg}$*;

1.471 at 1310 nm

1.470 at 1550 nm

Gbujhvf!Sftjtubodf!Qbsbnfufs!)o$_e$*;

20

Dpbujoh!Tusjq!Gpsdf;

Dry: 0.6 lbs. (2.7 N)

Wet, 14 days room temperature: 0.6 lbs. (2.7 N)

Approximation of Refractive Index Profile

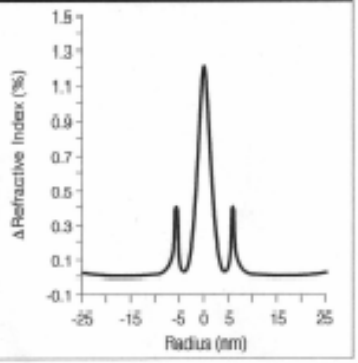

Spectral Attenuation (typical fiber)

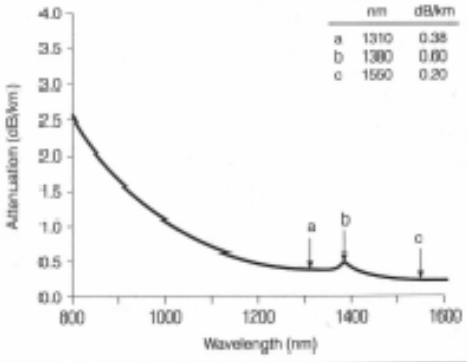

Ordering Information

To order Corning® SMF-LS™ CPC6 optical fiber, contact your sales representative, or call the Telecommunications Products Division Customer Service Department at : 21.4: 6.876: (in North America) and 718.: 85.8285 (outside of North America). Please specify the following parameters when ordering.

Fiber Type: *Corning® SMF-LS™ non-zero dispersion-shifted single-mode fiber*

Coating: *CPC6 (245 ñm outside diameter)*

Fiber Attenuation Cell: _____ dB/km

Fiber Quantity: _____ kms

Other: *(Requested ship date, etc.)*

CORNING

Corning Incorporated
Telecommunications Products Division
Corning, NY 14831 USA
Tel: (910) 395-7659 (in North America
Fax: (910) 395-7286 (in North America)
Tel: (607) 974-5354 (outside of North America)
Fax: (607) 974-7041 (outside of North America)
Email: fiber@corning.com
Internet: www.corningfiber.com

Corning fiber is made in the USA.

Count on Corning® Fiber

REFERENCES

[1] M. Vasilyev and T. I. Lakoba, "All-optical multichannel 2R regeneration in a fiber-based device," Opt. Lett. **20**, 1458 (2005).

[2] O. Leclerc, B. Lavigne, D. Chiaroni, and E. Desurvire, "All-optical regeneration: principles and WDM implementation," in *Optical Fiber Telecommunications IVA*, I. P. Kaminow and T. Li, Eds., Academic Press, San Diego, 2002, pp. 732−783.

[3] P.V. Mamyshev, "All-optical data regeneration based on self phase modulation effect," *24th European Conference on Optical Communication* (Institute of Electrical and Electronics Engineers, 1998), Vol.1, pp. 475−476.

[4] G. P. Agrawal, *Fiber Optic Communication Systems*, 3rd ed., Wiley & Sons, New York, 2002.

[5] A. Mahapatra and E. J. Murphy, "Electrooptic modulators," in *Optical Fiber Telecommunications IVA*, I. P. Kaminow and T. Li, Eds., Academic Press, San Diego, 2002, pp. 258−294.

[6] E. L Wooten, K. M. Kissa, A. Yi-Yan, E. J. Murphy, D. A. Lafaw, P. F. Hallemeier, D. Maack, D. V. Attanasio, D. J. Fritz, G. J. McBrien, and D. E. Bossi, "A Review of Lithium Niobate Modulators for Fiber-Optic Communications Systems," IEEE J. Sel. Top. Quantum Electron. **6**, 69 (2000).

[7] J. Zyskind, R. Barry, G. Pendock, M. Cahill, and J. Ranka, "High-capacity, ultra-long-haul networks," in *Optical Fiber Telecommunications IVB*, I. P. Kaminow and T. Li, Eds., Academic Press, San Diego, 2002, pp.198−231.

[8] P. J. Winzer and R.-J. Essiambre, “Advanced Optical Modulation Formats,” Proc. of the IEEE **94**, 952 (2006).

[9] J. DeAndrea, “Simplifying NRZ-to-RZ Conversion for Metro Designs,” CommsDesign, March 2, 2005, http://www.commsdesign.com/design_center/opticalnetworking/design_corner/showArticle.jhtml?articleID=60404548

[10] J. C. Mauro, S. Raghavan, and S. Ten, “Generation and system impact of variable duty cycle α-RZ pulses,” J. Opt. Commun. **26**, 1015 (2005).

[11] SHF Communication Technologies, Tutorial Note #5 “Modulation Schemes,” http://www.shf.de/en/communication/downloads/tutorial_notes/

[12] G. P. Agrawal, *Nonlinear Fiber Optics*, 3rd ed., Academic Press, San Diego, 2001.

[13] H. R. Sahu, S. Kant, “Enhanced bend insensitive high effective area NZDS fiber,” in *Proceedings of International Conference on Optics and Optoelectronics*, December 12−15, 2005, http://www.sterliteoptical.com.

[14] A. E. Willner and B. Hoanca, “Fixed and tunable management of fiber chromatic dispersion,” in *Optical Fiber Telecommunications IVB*, I. P. Kaminow and T. Li, Eds., Academic Press, San Diego, 2002, pp. 642−724.

[15] J. E. Hurley, “Setup and operation of a recirculating loop in a fiber-optic transmission system,” Corning Inc.’s internal report, 2000.

[16] R. Hesse and I. Tomkos, “Operational principles and realization of the recirculating loop testbed,” Corning Inc.’s internal report, 2001.

[17] M. Vasilyev and T. I. Lakoba, “Fiber-based all-optical regeneration of multiple WDM channels,” *Optical Fiber Communications* conference 2005, paper OME 62.

BIOGRAPHICAL INFORMATION

Pallavi received her Master of Science in Electrical Engineering from The University of Texas, Arlington in August 2006. She was born in Kolhapur, Maharashtra, India. She received her Bachelor of Engineering degree from Basaveshwar Engineering College, Bagalkot, India. Her research interests include optical communication and semiconductor device fabrication.